Open clusters and HII regions of our Galaxy

Willice Odhiambo Obonyo

August 2015

A project submitted in partial fulfilment of the requirements for the degree M.Sc. in the Department of Astronomy, as part of the National Astrophysics and Space Science Programme
UNIVERSITY OF CAPE TOWN

Supervisor: Dr Vanessa McBride

Abstract

Open clusters are essential laboratories for understanding stellar evolution, as they allow constraints to be placed on stellar ages and luminosities. As distance indicators they are also important tracers of star formation in the Milky Way. One such cluster is Trumpler 27 that we identified for detailed study.

The aim of the study is to estimate the distance, radial velocity, age, membership and reddening of the cluster using both spectroscopic and photometric techniques.

We used new spectroscopic data collected from SAAO's 1.9m telescope together with existing photometric data from catalogues in the study of Trumpler 27. The spectra collected were classified using spectral atlases to determine the reddening in the field. Stars of the cluster were identified using selection techniques that made use of both infrared and optical Q parameters, spatial distribution and photometric techniques.

The result from this work suggest that Trumpler 27 is made up of ~ 55 stars which are at different stages of evolution. The stars include main sequence stars, blue supergiants, two cool supergiants and maybe two WR stars.

The cluster's age and distance were found to be $\sim 10^{7.0\pm0.2}$ years old and $\sim 2.6 \pm 0.2$ kpc away from the sun respectively. It is therefore located on the outer part of Scutum Centaurus arm of the Galaxy. Its reddening, $E(B-V)$ varies substantially across the field with the average value being $\sim \ 1.3 \pm 0.2$. The radial velocity of the cluster was estimated as the average value of radial velocities of its cool supergiants which is $\sim 18.5 \pm 2.3$ km/s. During selection process, another population of younger OB stars that is ~ 3.5 kpc away from the sun and is right behind Trumpler 27 was identified. This group maybe a cluster or just background stars that look like a cluster.

Acknowledgements

I want to acknowledge SKA for funding the work, Dr. McBride for supervision and SAAO for observing time on the 1.9m telescope.

Plagiarism Declaration

I, Willice Odhiambo Obonyo, know the meaning of plagiarism and declare that all of the work in the document, save for that which is properly acknowledged, is my own.

Contents

List of Figures

List of Tables

Chapter 1

Introduction

Open clusters are useful in the study of stellar evolution, estimating Galactic distances and tracing star forming regions. They are made up of massive stars ($M > 8M_{\odot}$) which are characterised by higher luminosities and temperatures compared to low mass ones. Their stars are good ionisers of the interstellar medium (ISM) and chemical enrichers of the Galaxy. The ionised ISM re-radiates at longer wavelengths giving information about its properties and structure (Reynolds et. al 2008).

Apart from open clusters, there are also globular clusters which are older, more spherical in shape and have higher stellar densities. The diffuse nature of open cluster stars make it easier to resolve and observe them individually compared to globular cluster ones.

Open clusters are younger compared to globular ones. The average age of an open cluster is $\sim 10^8$ years (Dias et al. 2002) but some of them are as young as $\sim 10^6$ to as old as $\sim 10^{10}$ years (Binney & Merrifield 1998, Dias et al. 2002) e.g Berkeley 17 and ESO 311 21 whose ages are estimated to be $\sim 10^{10}$ (Gozha et al. 2012) and $\sim 10^{10.1}$ years old respectively (Dias et al. 2002).

The average size of an open cluster is $\sim 4-5$ pc but some are as small as 1 pc while others are as wide as 20 pc. Stars in a cluster can be spread over a considerable part of the sky making it difficult to identify them from foreground/ background stars in the field.

The clusters can be classified as embedded or non embedded depending on the amount of gas around them. Embedded clusters are those that are partially or fully immersed in interstellar dust. Such clusters are invisible at optical wavelengths because they are covered by large amounts of dust. This study is based on non embedded clusters since the amount of ISM around them allows for their study at optical wavelengths.

Open clusters are surrounded by regions of ionised hydrogen gas called HII regions. The HII regions are ionised by early type stars of the clusters. These regions are the most luminous objects in the Galaxy at the mid-infrared and the radio wavelengths (Balser et al. 2011). This property makes them better Galactic distance estimators of dusty parts of the Galaxy compared to open clusters.

Dust particles between an observer and a star makes the star appear redder and fainter.

The correct colour and magnitude of a star is therefore estimated by dereddening the apparent colour of a reddened star and subtracting visual extinction from its apparent visual magnitude. Once a star is dereddened and its magnitude correctly estimated, the position of the star in a HR diagram can be determined.

This thesis is based on spectroscopic and photometric study of open cluster Trumpler 27. The cluster has both young and rare older stars making it a good laboratory for study of massive stellar evolution. The stars include main sequence (MS) stars, blue supergiants, cool supegiants and the very rare Wolf Rayet stars. We employed a detailed selection procedure using reddening free parameters in identifying Trumpler 27 stars for spectroscopic and photometric study. Spectroscopy was used for a number of purposes such as estimating cluster reddening and to specifically search for the cluster's MS stars which is lacking in previous studies.

Other causes of interest in the cluster are its distance, existence and reddening. Different authors have given different distance estimates for the cluster with the nearest estimate being 0.8 kpc (The & Stokes 1970) and the farthest $\sim$ 2.5 kpc (Massey et al. 2001). Perren et al. (2012) and Imhoff & Keenan (1976) do not believe that Trumpler 27 is a cluster. Perren et al. (2012) concluded that there may be two or more clusters along the cone of sight of the cluster. They noticed a region of stellar over density at a distance of $\sim$ 3.5 kpc in the direction of the cluster. The heavy and variable reddening across the cluster has been cited as the major cause of confusion about its distance and existence. Details about literature on star clusters, methods used, results obtained and and conclusion are given in the next five chapters of the work.

The thesis is divided into five chapters. Chapter one of the report gives a brief overview of the work and the objectives of the study. In chapter two the literature about massive stars, HII regions, open clusters, spectroscopy and Galactic structure is given. Chapter three is about the methods used in data collection, reduction and analysis while in chapter four, the results are presented together with a discussion on the result. Lastly chapter five is about conclusions made from the results discussed and recommendations for future work in star clusters in general and Trumpler 27 in particular.

1.1 Objectives of study

The objective of the study are:

1. To identify bright stars in Trumpler 27 field for spectroscopic study.
2. To estimate extinction, distance, radial velocity and age of Trumpler 27
3. To establish, if any, the relationship between the blue supergiants, cool supergaints and Wolf Rayet stars in the field of Trumpler 27.
4. Use HII regions from HRDS (HII regions discovery survey) and Sh2 catalogues to search for poorly studied open clusters that are optically visible.

Chapter 2

Background

2.1 Star clusters

A star cluster is a group of stars that is gravitationally bound together. The stars can be found in binaries, triple systems or in larger groups of ~ 10 or more stars. Stars in a cluster have a common age, centre of gravity, distance and chemical composition (Goetz 1991). Nearly all stars do not form in isolation but in groups. The stellar densities of the groups range from as low as $\sim$10 stars per cubic parsec to as high as $\sim$ 100 stars per cubic parsec or more in regions of higher stellar densities (Kirk et al. 2014).

A cluster is either stable or unstable based on its stellar density and velocity dispersion. A cluster is said to be stable if it has 35 or more stars and a mass density $> 1 M_{\odot} pc^{-3}$. Velocity dispersion of stars in a cluster also gives information about its stability with stars of stable clusters having smaller velocity dispersion compared to those of unstable ones. A stable cluster is able to live for at-least $\sim 10^8$ years before its members diffuse out completely (Lada & Lada 2003).

Some clusters are easier to identify in a field of stars since they show higher concentration on a smaller part of the sky (Figure 2.1). The difficulty in identifying a cluster varies with its stellar density and effect of background stars. The higher the density of a cluster the easier it is to identify. This explains why globular clusters (see Figure 2.2) which are more compact and spherical are easier to identify compared to their open counterparts.

Identifying stars of an open cluster in a crowded field is tricky and the best parameter to use is the radial velocities of the stars. This works best since RVs of stars in a cluster have limited velocity dispersion around the cluster's peculiar velocity.

2.1.1 Globular and Open clusters

Globular cluster

Globular star clusters are spherically shaped collections ($\sim$ hundreds of thousands) of densely populated stars. They are strongly bound gravitationally and have longer lifespans, with the

Figure 2.1: Stars of open clusters concentrated on small parts of the sky. The image is for open clusters NGC 884 on the left and NGC 869 on the right (Nemiroff & Bonnell 1995).

youngest estimated to be $\sim$ 10 billion years old. They are quite important in constraining the lower limit of the universe's age since they are the oldest objects in the universe. The clusters lack OB stars because they are too old (Binney & Merrifield 1998).

Figure 2.2: The Messier 80 globular cluster in the constellation Scorpius. It is located about 28,000 light-years away from the Sun (Nemiroff & Bonnell 1995).

Open clusters

An open cluster is a diffuse collection of gravitationally bound stars that was born from a single giant molecular cloud (GMC). They are mostly found in the Galactic disc from where they derived their common name - Galactic clusters. The clusters may be highly obscured due to their location (Galactic plane).

An open cluster may contain as few as $\sim$ 10 to as many as thousands of stars. The stellar densities in these clusters range from $\sim 0.1 - 10^3$ stars per cubic parsec. The density within

a cluster also varies with the inner part, where gravitational effect is strongest (called the core), having the highest density. The core has a radius of $\sim 1-2$ pc. The region outside the core, called tidal region, has lower stellar density. The outer region lie within a radius ranging from $r \sim 3-4$ to $10-20$ pc (Binney & Merrifield 1998). The clusters are normally surrounded by gas remnants from GMCs. The gases are ionised by the young early type (OB) stars in the cluster resulting in HII regions around them.

Figure 2.3: Left: Non embedded open star cluster NGC 3572 and its surroundings (www.scitechdaily.com). Right: Embedded open star cluster NGC 2175.

Stars within a cluster may have different ages but the age difference between stars in a cluster is small compared to the time taken to form the cluster. This means that all the stars in a cluster can be considered to have the same age (Elmegreen & Efremov 1998).

2.1.2 Star cluster formation

The observational study of formation of globular clusters is impractical because they are too old ($\sim 10-13\times10^9$ years). These clusters are almost as old as the universe itself (Karttunen et al. 2007) making it difficult to gather facts about their formation observationally (Massey 2003). There are though new observational ideas about their formation (Ashman & Zepf 2001) such as young massive clusters showing properties suggesting that they might evolve to become globular clusters (Zhao 2007).

Open clusters on the other hand are younger and their formation processes are ongoing in the GMCs. Formation of stars in open clusters starts when GMCs fragment (Figure 2.4) into clumps. The clumps form due to variation in density, particle size and temperature within the GMCs. When the number densities of the clumps/cores exceed 10^4cm^{-3}, they collapse to form stars (Lada & Lada 2003).

The cores/clumps are denser compared to other parts of the clouds making them to accrete more materials. The accretion of materials induce temperatures rise in the cores which result in outward radiation that drives away gas surrounding the stars. As more stars in the clouds are being born, a cluster is formed. The clusters formed have a number of properties such as size, gravity, lifespan and stellar density. The properties vary depending on the initial size and feature of the mother GMC.

Figure 2.4: Left: A computer simulation illustrating how GMCs fragments. Right: A picture of stars formed from GMCs (Elmegreen & Efremov 1998).

2.1.3 Cluster lifespan

Lifespan of a cluster depends on its gravitational strength, environment and velocity dispersion of its stars. If the gravitational pull of a cluster is high enough to hold its members with little disruption then it lives longer. A cluster located near massive objects, e.g GMCs, is likely to be disrupted by tidal effects compared to an isolated one.

The length of time for which a star remains bound to its cluster depends on the gravity of the cluster and its velocity relative to that of a cluster. Stars in a cluster move away from the cluster's centre of mass (CM) gradually as they lose material through winds. This is because as the stars lose materials, the gravitational attraction between them and the cluster's CM weakens leading to diffusion of the stars and eventually expansion of the cluster.
Clusters can also diffuse though a process called gravothermal catastrophe (O'Leary et al. 2014). In this method, binary systems are said to form in the cluster cores. The systems then generate heat that is enough to heat up the entire cluster making it expand.

Most open clusters do not remain in bound state for long (up to $\sim 10^8$ years). They interact with other systems as they move about in the fields resulting in their distortion. Once distorted, the open cluster allow its stars to escape from its gravitational field.

2.1.4 Hertzsprung-Russell (HR) diagram

HR diagram is a tool for analysing photometric data of stars. It is a diagram (Figure 2.5) that uniquely positions a star based on its temperature and luminosity. The hot and luminous stars position themselves on the top left corner of the diagram while the cooler and less luminous ones go to the bottom right corner.

Main Sequence stars form a mass dependent pattern that run diagonally from top-left to bottom-right part of the HR diagram (Figure 2.5). The supergiants arrange themselves horizontally across the diagram on the upper part. The SGs maintain their luminosity even if they are cooler because of their large sizes. Giant stars on the other hand branch from the MS diagonally towards the top right part where they form the red giant branch.

Instead of a luminosity-temperature graph, a similar diagram called colour magnitude

diagrams (CMD) can be used. In the CMD, the luminosity and temperature axes of HR diagram are replaced with the magnitude and colour axes respectively. CMDs are easy to make once photometric data of stars are made available.

A typical CMD of an open cluster is broader at the base of the MS and narrower at the top. This is because massive stars evolve faster and go off the MS while the low mass ones are still moving towards it.

HR diagrams of open and globular clusters differ in structure as shown in Figure 2.5. An open cluster HR diagram is dominated by OB stars while that of a globular cluster is missing O, B, A and even F stars. A globular cluster diagram is dominated by cooler red giants. The brightest members of a globular cluster are found on the tip of the red giant branch or asymptotic giant branch (Karttunen et al. 2007).

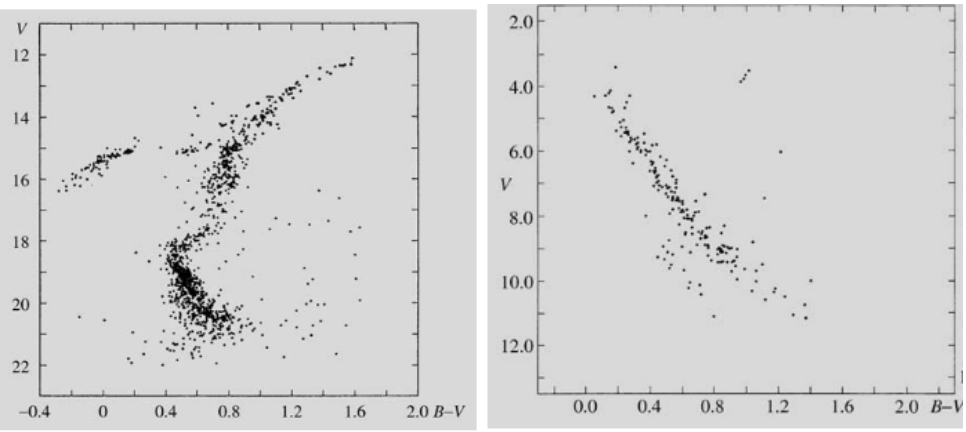

Figure 2.5: Left: CMD of globular cluster M5. Right: CMD of open cluster Hyades. The distance moduli of Hyades and M5 are 3.3 (van Bueren 1952) and 14.39±0.1 (Coppola et al. 2012) respectively. Illustrations taken from (Karttunen et al. 2007).

2.1.5 Importance of studying star clusters

Distance estimators

Star clusters cover a small part of the sky compared to their distances from the earth. This means that stars of a cluster are at a common distance from us. If distances to different Galactic clusters are accurately estimated, then the Galaxy map can be improved.

The distance to a cluster can be estimated from its CMD. The CMD should be for its members only since contaminants complicate MS fitting. The colours and magnitudes of the stars are corrected for extinction before they are used in making the CMDs. An example of a CMD of two clusters (Pleiades and Hyades) is shown in Figure 2.6. The illustration was taken from `http://cse.ssl.berkeley.edu/bmendez/ay10/2002/notes/lec17.html`.

Figure 2.6 shows that Pleiades is 7.5 times fainter than the Hyades cluster. The distance, d to one of the clusters can be estimated if distance of the other is known using the equation:

$$\text{Flux (brightness)} = \frac{\text{Luminosity}}{4\pi d^2} \tag{2.1}$$

In magnitudes,

$$m - M = 5 \log d - 5 \tag{2.2}$$

Where M, m and d are the absolute magnitude, apparent magnitude and the distance to the cluster in pc respectively.
The methods are only practical if distance to a reference cluster is known. A nearby reference cluster can be calibrated using MS of stars within the solar neighbourhood whose distances can be estimated accurately using parallax or moving cluster method (Binney & Merrifield 1998). In this work, MS of stars at a distance of ∼10pc from the earth have been used as a reference (Drilling & Landolt 2000, Mermilliod 1981) group.

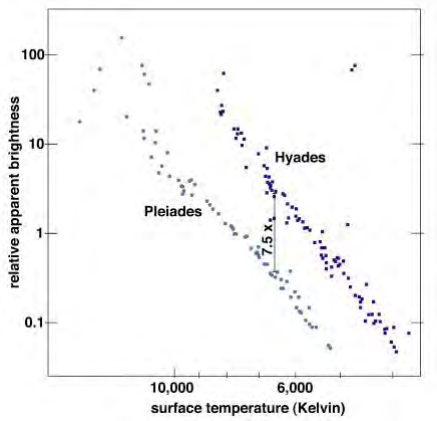

Figure 2.6: CMD for open clusters Pleiades and Hyades.

Age estimators

The age of an open or globular cluster can be estimated from their CMD. There are theoretical models of stellar evolution that can be used to estimate age of a cluster. The models are based on masses, metallicities, opacities, rotation speed among other properties of stars. Massive stars evolve faster than low mass ones causing them to leave MS earlier.

The evolution models were used by Bressan et al. (2012) and Ekstrom et al. (2012) to come up with curves representing coeval stars called isochrones (Figure 2.7). The isochrones can be fit to data-points of a cluster's CMD in order to estimate its age.

The age of a cluster is estimated from its MS turnoff (MSTO). A star's turn-off point is a stage when its hydrogen is exhausted in its core. At this point, hydrogen, which is the main fuel, is being burnt in the shell around the core. A turn-on, which is the time stars begin to join MS and corresponds to the start of nuclear fusion in the core can also be used to estimate a cluster's age. Both turn-off and turn-on can be used together to improve the accuracy of the age estimated.

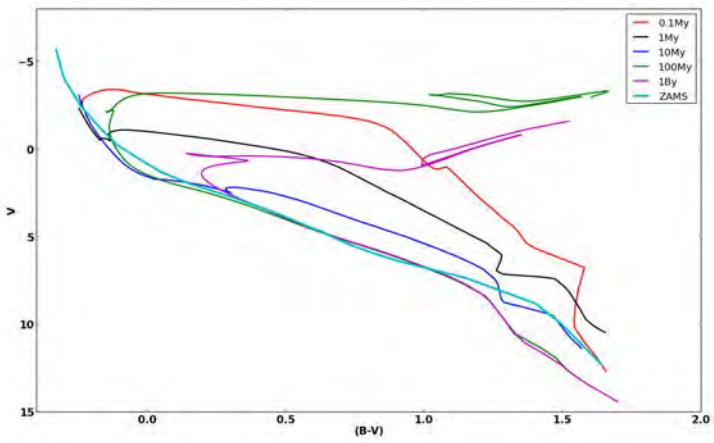

Figure 2.7: PARSEC (Padova And TRieste Stellar Evolution Code) isochrones (Bressan et al. 2012) of different ages. ZAMS (Drilling & Landolt 2000) of stars is shown in cyan. Some stars are evolving off the MS while others are evolving towards it.

From the modelled isochrones, it is clear that a cluster whose age $\sim 10^5$ years has a shorter MS compared to an older one. Older clusters ($\sim 10^8 - 10^9$ years) on the other hand have more low mass stars on the MS compared to their high mass ones which have evolved off MS. Age of a cluster can also be estimated using equation 2.3 if its turn off and metallicity are known (Binney & Merrifield 1998):

$$\mathrm{M_V(TO)} = 2.7 \log(\frac{t}{\mathrm{Gyr}}) + 0.3[\mathrm{Fe/H}] + 1.4 \tag{2.3}$$

Where M_V is the absolute magnitude corresponding to turn-off point, t is the time in Gyr and [Fe/H] is cluster metallicity. Metallicity is the fraction of chemical elements heavier than helium in an astronomical object. The sum of fractions of hydrogen (X), helium (Y) and metals (Z) in an object is one i.e $X + Y + Z = 1$

Understanding Evolution of stars

Stars live for millions to billions of years and monitoring them from birth to death in a man's lifetime is impossible. The evolution pattern of stars can be inferred after studying a number of clusters of various ages. The changes in clusters as they age out can be noted and used in designing an evolution theory for the stars.

There are three major stages of evolution of stars namely: pre-main sequence, main sequence and post main sequence. The time taken by a star to evolve is governed by its initial mass ($t_n \sim 10^{10} \times (\frac{M}{M_\odot})^{-2.5}$, where t_n is the lifetime of a star) years (Padmanabhan 2001). Table 2.1 shows one of the proposals of evolution patterns of massive stars.

Table 2.1: Summary of massive star evolution (Maeder & Meynet 1987).

Initial Mass ($M_\odot$)	Evolutionary Sequence	Supernova Type
50+	O → Of → BSG → LBV → WR	Ib
30 - 50	O → BSG → YSG → RSG → WR	Ib
10 - 30	O → RSG	II-P

Key:

O	O-type main sequence star
Of	Evolved O-type showing N and He emission
BSG	Blue supergiant
RSG	Red supergiant
LBV	Luminous blue variable
WR	Wolf-Rayet star

Estimating extinction to a cluster

Dust particles scatter (and absorb) light passing though them. This makes star light to appear redder and fainter as shown on Figure 2.8. To estimate the true colour and magnitude of a star, reddening and extinction corrections must be done. The reddening value can be estimated as the difference between observed and intrinsic colours of a star. The intrinsic colours of spectroscopically observed stars can be inferred from their spectral classes (Fitzgerald 1970) while those of other stars in the field can be estimated from a reddening free quantity, called Q parameter (Johnson & Morgan 1953). Mathematically the optical colour excess (also known as reddening), $E(B-V)$ is given as:

$$E(B-V) = (B-V)_{observed} - (B-V)_{intrinsic} \tag{2.4}$$

The stellar flux lost when its light is scattered or absorbed can be expressed in magnitudes as:

$$A_V = V - V_o \tag{2.5}$$

where A_V, V and V_o are called visual extinction, apparent visual magnitude and intrinsic visual magnitudes respectively.

Reddening/ extinction of objects depends on amount of dust particles along the line of sight and the wavelength of the radiation (Figure 2.8). The shorter the wavelength of light the higher the extinction, A_λ (Cardelli et al. 1989) it experiences. Objects that lie on the Galactic plane suffer more extinction since the photons from them pass through a number of dust rich spiral arms before reaching an observer.

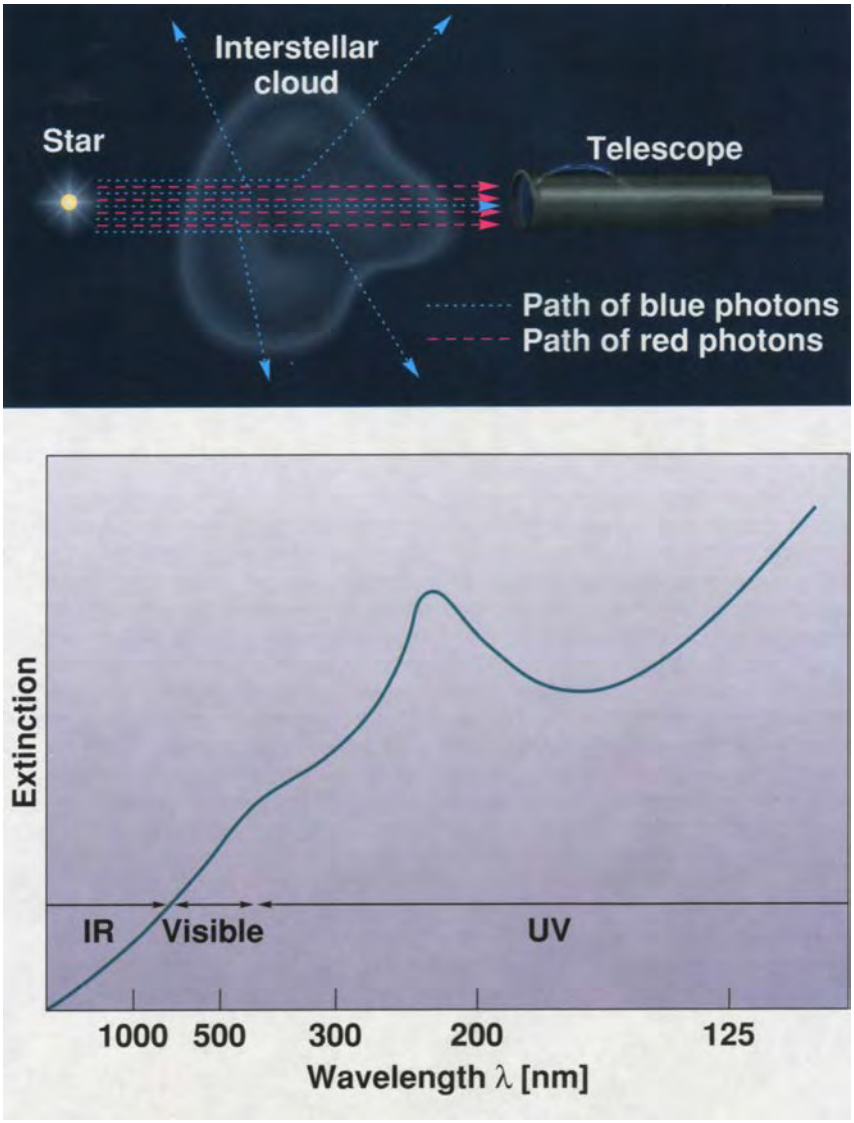

Figure 2.8: A schematic diagram illustrating extinction process on the upper part. The lower part illustrates how extinction varies with wavelength. Image taken from http://crab0.astr.nthu.edu.tw/ hchang/ga2/ch25-01.htm.

The ratio of total, A_V to selective $E(B-V)$ absorption of objects a constant, R_V.

$$R_V = \frac{A_V}{E(B-V)} \tag{2.6}$$

This ratio, R_V is ~ 3.1 in cases of standard reddening but this can change depending on the colour of a star ($R_V = 3.2 + 0.21 \times (B-V)_0$ Celis 1981, Jackson et al. 1980) and characteristics of dust particles.
In a cluster, R_V can be estimated from a $V - M_v$ vs $E(B-V)$ plot (Figure 2.9). The gradient of the plot gives intra-cluster reddening constant, R_V (see equation 2.8).

$$V - M_V = 5\log \mathrm{d} - 5 + A_V \tag{2.7}$$

$$V - M_V = 5\log \mathrm{d} - 5 + R_V E(B-V) \tag{2.8}$$

where V and M_V are the apparent and absolute magnitudes of stars.

This graph can also be used to estimate distance to a given cluster if the least reddened star in the cluster is identified correctly. The distance modulus (DM) of a cluster is given by the y-intercept of a standard law drawn from the least reddened star in the plot (Figure 2.9). This method is more reliable when there is a good range in $E(B-V)$ i.e variable extinction in a cluster.

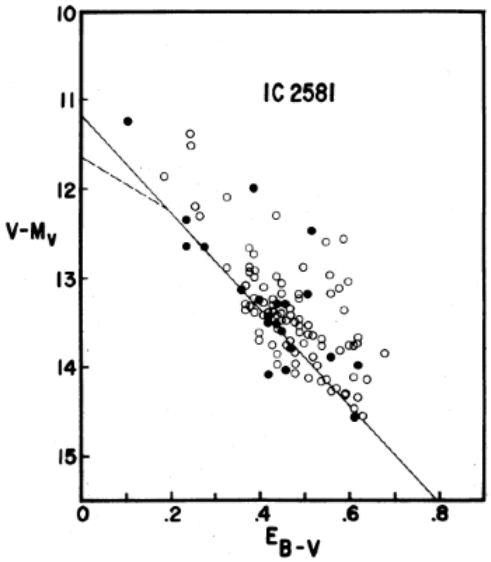

Figure 2.9: $V - M_V$ vs $E(B-V)$ plot of open cluster IC2581 stars. The closed and open symbols represent photoelectric and photographic data of cluster stars respectively. The solid line is a fit on the lower envelope of cluster members while the dotted one is a standard reddening line constrained by the least reddened member(s) of the cluster (Turner 1973).

2.1.6 Infrared study of open clusters

Infrared light ($\sim$ 0.75 to 300μm) enables us to pierce through interstellar dust, which blocks visible light. The light is less affected by dust and it allows us to see objects at extreme cosmological distances e.g galaxies in the early universe.

There are $\sim$ 1800 known open clusters while estimates put the total number of the clusters in the Galactic disc to be $\sim 10^5$ (Sung 2006). The low number of known clusters is due to the fact that their search has been done predominantly in the optical wavelength. With the availability of NIR data in 2MASS catalogue, more clusters which cannot be identified in the optical can be discovered in the NIR. JHK$_s$ band wavelengths are J(1.25μm), H(1.65μm) and K$_s$(2.16μm).

The discovery of 96 new infrared open clusters and stellar groups by Borissova et al. (2011) confirms the importance of studying clusters using IR wavelength. Their use of VVV (VISTA Variables in the Vía Láctea) survey (Minniti et al. 2010) data revealed that IR images show over-density where shorter wavelength bands fail (see Figure 2.10). Recent work by Camargo et al. (2015) where they studied embedded clusters using WISE data whose images are in the wavelengths of 3.4, 4.6, 12 and 22 μm also confirm that IR wavelengths can study the highly optically obscured embedded clusters.

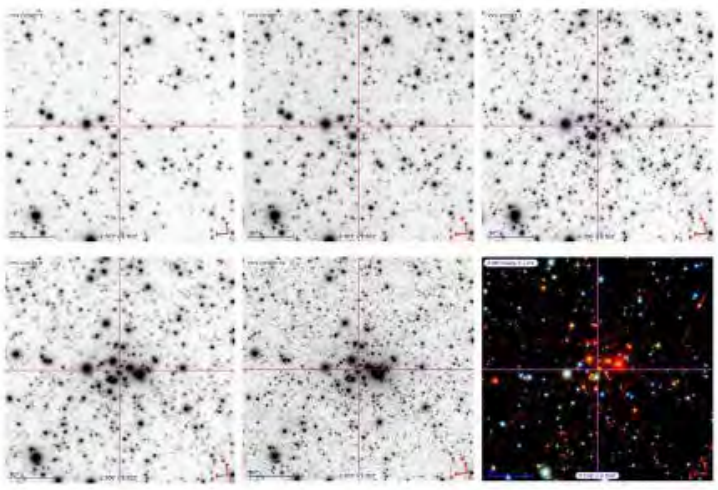

Figure 2.10: The VVV $ZYJHK_S$ images and ZJK_S true colour image of VVV CL036. The field of view is 2.5 $\times$ 2.5 arcmin, North is up, East to the left (Borissova et al. 2011).

2.2 Spectroscopy

2.2.1 Introduction

Stars can be classified using their temperature, colour, mass, spectral type, proper motion, radial velocity, radius among other features (Jaschek & Jaschek 1987). The most commonly

used method of stellar classification is using a spectrum that estimates its temperature and luminosity. Spectral features of the spectra are used to sort stars into groups called spectral classes. Absorption and emission lines are the main features used in classifying the spectra (Carroll & Ostlie 2006). An image showing a spectrum on a CCD camera is as shown on Figure 2.11.

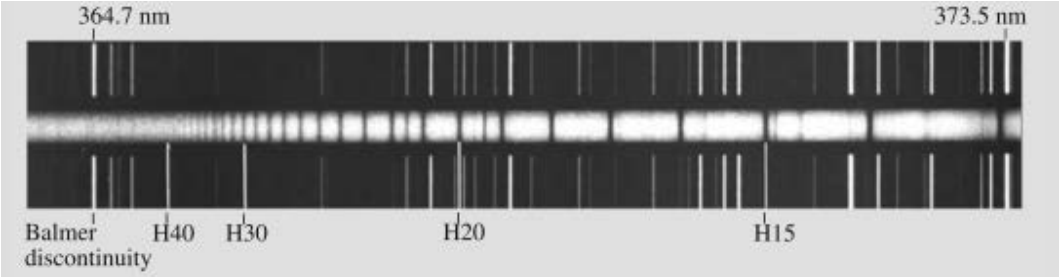

Figure 2.11: An illustration of a spectrum. The white strip with small vertical lines show a continuum in white and absorption lines in black. The other two darker parts on either side of the bright strip show emission lines on a continuum (Karttunen et al. 2007).

2.2.2 Spectral classification

Spectral classification is done by identifying lines present in a spectrum and calculating line ratios of some lines. Spectral line strengths change with temperature (2.12). Instead of line strengths, line ratios are used since they are independent of continuum calibration. The line strengths/ratios also play a role in luminosity classification.

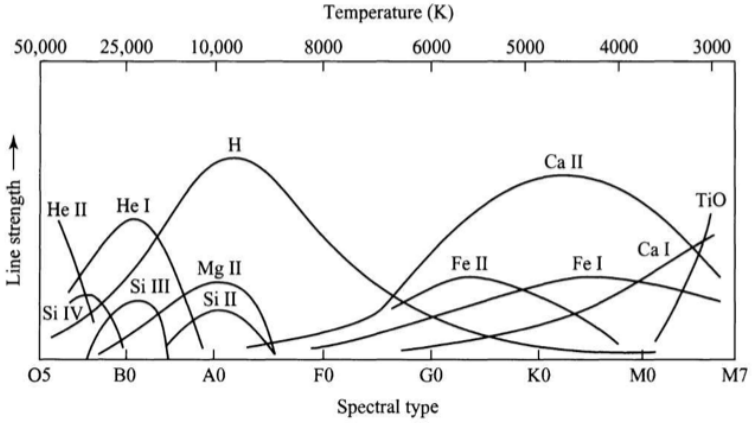

Figure 2.12: Changes in line strengths with spectral class (Carroll & Ostlie 2006).

HeII lines are the strongest in O stars (Figure 2.12) followed by HeI lines which are strongest from $\sim$ O8 to $\sim$ B5. HI, CaII and TiO lines are the strongest line between B5 - F8, F8 - M4 and late M stars respectively (Carroll & Ostlie 2006). The kind of lines present

in a spectrum depends on the temperature of the star observed. Table 2.2 gives a summary of spectral class and the prominent lines in the class.

Table 2.2: Spectral classes and prominent absorption lines in the classes Carroll & Ostlie (2006)

Spectral Class	Intrinsic colour	Temperature (K)	Prominent Absorption Lines
O	Hottest Blue-White	30000-60000	Strong HeII, HeI, HI, OII, NII, SiII
B	Hot Blue-White	10000-30000	HeI strongest at B2, HI lines becoming stronger
A	Blue-White	7500-10000	H(strongest), CaII, MgII, FeII
F	White	6000-7500	HI (weaker), CaII, ionized metals
G	Yellow-White	5000-6000	HI (weaker), CaII, ionized and neutral metal
K	Orange	3500-5000	CaII (strongest), neutral metals strong, HI (weak)
M	Red	< 3500	Strong neutral atoms, TiO I

A star is classified fully by using its spectral class and luminosity class. Luminosity class gives information about the size of the star. There are eight luminosity classes as shown in Table 2.3. These luminosity classes are part and parcel of spectral classification and are used together.

Table 2.3: Luminosity classification of stars (Leblanc 2010).

Luminosity Class	Symbol
Bright supergiants	Ia
Supergiants	Ib
Bright giants	II
Giants	III
Subgiants	IV
Dwarfs (Main sequence)	V
Subdwarfs	VI
White dwarfs	VII

2.2.3 Spectral line features

Spectral lines differ in terms of width and intensity. The changes in strength of lines can be computed mathematically as equivalent widths (see Figure 2.13). Equivalent width is the width of a rectangle whose area is equivalent to the area of a spectral line. The height of the rectangle is the same as the height of the continuum. The width is related to strength of a spectral line. Rotating stars, those with higher temperature and atmospheric pressure have broader lines e.g dwarfs.

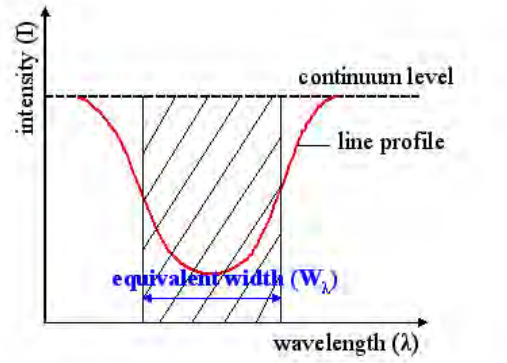

Figure 2.13: Equivalent width of an absorption line.

Chapter 3

Cluster search

3.1 Search from HII regions

We searched for new clusters from HII regions in Sh2 (Sharpless 1959) and HRDS (HII Region Discovery Survey Bania et al. 2010) catalogues. This was done by identifying HII regions that are not already associated with optically visible open clusters (Dias et al. 2002). We took 2MASS data of the point source objects in the fields and used them to make K vs Q_{IR} and K vs $(J-K)$ plots (as in section 4.1). Surface density and IR magnitude distribution plots were made in-order to identify regions of higher concentration. If a region of higher stellar concentration was noted then follow up was done.

An over-plot of HII regions and optically visible open clusters (Dias et al. 2002) was used to identify HII regions which do not have known open clusters as shown in the Figure 3.1. The plots revealed that there are a number of HII regions that do not have known open clusters. The HII regions may have unknown infrared open clusters (Kronberger et al. 2006).

HII regions that are close to the Galactic plane were discarded since they suffer high extinction. This left us with ∼70 HRDS HII regions that lie $\sim 0.5^o$ away from the Galactic plane. Of the ∼70 regions, ten lie between $l = 340^o$ and $l = 360^o$, which is the area we were interested in mapping using clusters. Six regions out of the ten (shown in Figure 3.2) have the largest angular distance with their nearest neighbours and were the ones identified as the best candidates in studying the region. Their names and co-ordinates (J2000) are shown on Table 3.1:

The regions were selected on the ground that they are at least $\sim 0.2^o$ away from the nearest cluster or HII region. This is the average distance considered to be sufficient to accommodate two clusters sideways without overlapping. The average diameter of optically visible open clusters is $14'$ ($\sim 0.2^o$) meaning that the nearest distance between the centres of non overlapping clusters should also be $\sim 0.2^o$.

Some HII regions have very large diameters e.g Sh 2-257 whose diameter is 20^o. Such HII regions may contain multiple clusters. The wider HII regions were avoided since it is

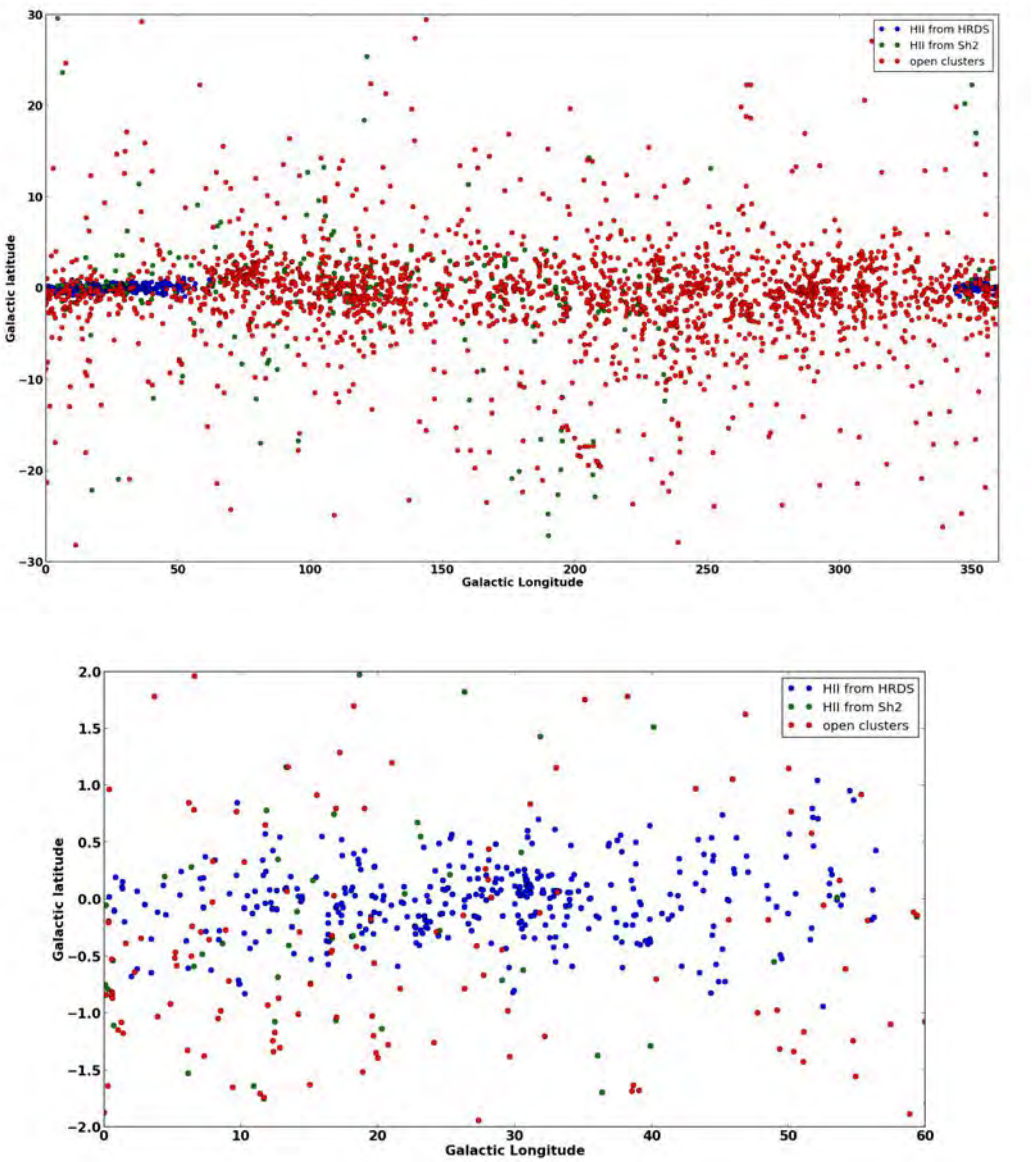

Figure 3.1: An over-plot of HII regions and optically visible open clusters. The plot on the bottom part is a zoomed section of the upper plot from latitude of $\sim -2^o$ to 2^o and longitude of $\sim 0^o$ to 60^o.

not easy to tell whether a cluster in its field is within the region or at the background.

Table 3.1: HRDS - HII regions selected

HII region	RA(J2000)	DEC (J2000)
G345.283−0.990	257.34	-41.7214
G358.379−0.840	266.2567	-30.7573
G344.106−0.672	256.0435	-42.4702
G354.979−0.528	263.8123	-33.4723
G351.359+1.014	259.8091	-35.6202
G351.265+1.019	259.7377	-35.6943

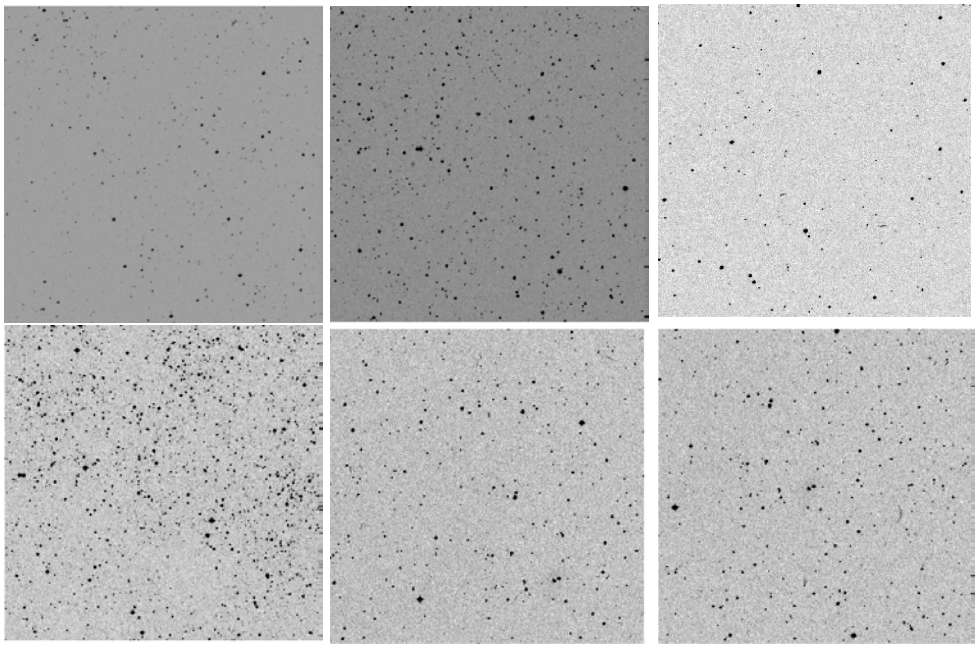

Figure 3.2: From top left, $G345.283-0.990$, $G358.379-0.840$, $G344.106-0.672$, $G354.979-0.528$, $G351.359+1.014$ and $G351.265+1.019$. $15'$ by $15'$ optical displays of the HII regions. North is on the upper part and East is to the right.

The regions identified do not show any clustering of infrared stars on their field by inspection and a plot of the surface density of their early type stars were made. Gomez et al. (1993) described a method that allows for estimating surface density of stars. The surface density is said to be $\sim 2-10$ stars/pc^2 for field stars and $\sim 10-20$ stars/pc^2 for a cluster. The formula used to estimate surface density, D, at a point on the sky (α, δ) from a weighted average of observed stellar density smoothed over length, h, is given as:

$$D(\alpha,\delta) = \frac{1}{h^2}\sum_{i=1}^{n} K(\alpha,\alpha_i,\delta,\delta_i) \text{ in number of stars/square degree} \tag{3.1}$$

The weighting is provided by the Kernel function, K given by Gaussian Kernel adopted by Gomez et al. (1993) as:

$$K(\alpha, \alpha_i, \delta, \delta_i) = \frac{1}{2\pi} e^{\frac{-r^2}{2h^2}} \tag{3.2}$$

where r is the separation of neighbouring stars, given as $r^2 = (\delta - \delta_i)^2 + (\alpha - \alpha_i)^2 cos^2\delta$ and α, δ & h are in degrees.

The result for HII region $G345.283 - 0.990$ obtained using the explained cluster search procedure is shown in figure 3.3. All the regions showed clustering behaviour from the surface density plots.

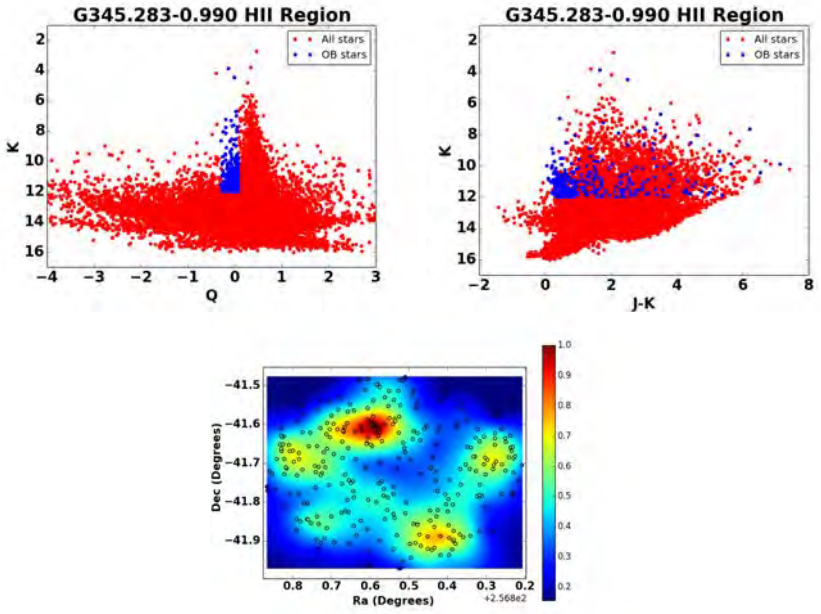

Figure 3.3: Illustrations showing K vs Q plot, K vs $J - K$ plot and a surface density map for early type stars in HII region $G345.283 - 0.990$

The identified HII regions have stars that are too faint to study optically using the 1.9m telescope that we could access. This forced us to study an already studied open cluster called Trumpler 27. This cluster was settled on because of the confusion surrounding its distance and existence.

3.2 Case cluster: Open cluster Trumpler 27

In this work we perform an in-depth study of open cluster Trumpler 27. This cluster is located at $l \sim 355.064^o$, $b \sim -0.742^o$ (Perren et al. 2012, Bakker & The 1983, Moffat et al. 1977). The distance to the cluster has been variously estimated (0.8 kpc to 2.5 kpc)

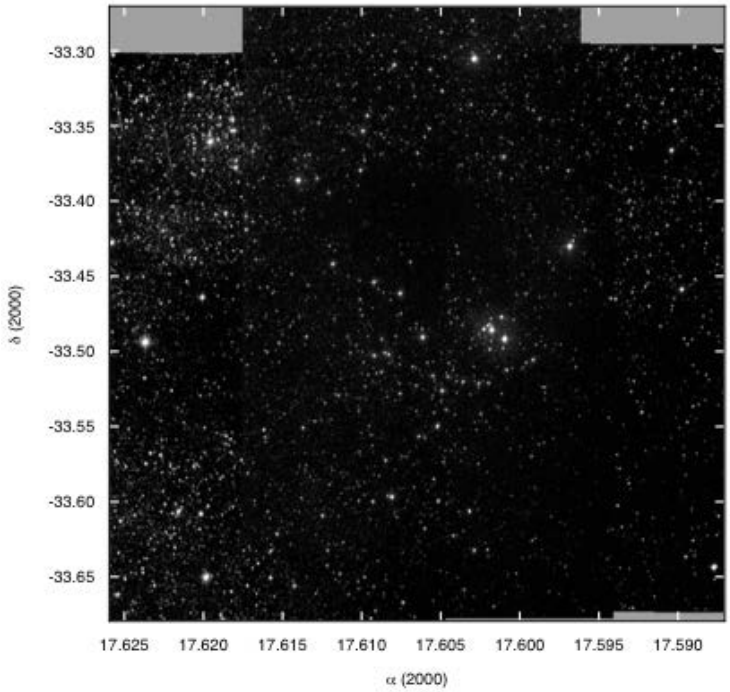

Figure 3.4: A 26′ by 23′ V image of Trumpler 27 field showing obscuration in the field. North is up, east is left (Perren et al. 2012).

by different authors. Bakker & The (1983), Moffat et al. (1977) and Massey et al. (2001) estimated its distance as 1.65 ± 0.25 kpc, 2.1 ± 0.2 kpc and 2.5± 0.3 kpc respectively. They all placed it on the Sagittarius arm. Perren et al. (2012), on the other hand, conclude that it is not a cluster. They concluded that there is a region of stellar over density in the direction of the field at a distance of ∼ 3.5 kpc. Perren et al. 2012 also suggest that if there is a cluster then it is not one but two or three overlapping each other within the cone of sight leading to the field.

An optical picture of the field (Figure 3.4) shows heavy obscuration forming a ring like pattern about the point $\sim \alpha = 17.605, \delta = -33.5(J2000)$, which is the perceived centre of this cluster.

The cluster is made up of a number of blue supergiants, one yellow supergiant, one red supergiant and two Wolf Rayet stars (Moffat et al. 1977). The size of Trumpler 27 is ∼ 8′ and contains between 50 to 60 members (Moffat et al. 1977, Bakker & The 1983). It is a young cluster whose age is $\sim 10^6 - 10^7$ years (Bakker & The 1983).

The cluster was studied by taking spectra of 19 stars in its field. The observations and the results from spectra are presented in the next chapter. These spectra allowed us to constrain the reddening to the cluster, which is used in Chapter five to estimate age and distance.

Chapter 4

Spectroscopic analysis of Trumpler 27

4.1 Target selection for spectroscopy

We selected the brightest OB candidate stars in the Trumpler 27 field from the 2MASS catalogue (Cutri et al. 2003). The stars selected are those whose $K_s \leq 11$ (brightest) and infrared reddening free parameter $-0.3 \leq Q_{IR} \leq 0.08$ (early type stars) (Negueruela et al. 2012, Ramírez Alegría et al. 2012). The infrared reddening free parameter is mathematically given as:

$$\mathrm{Q_{IR}} = (\mathrm{J} - \mathrm{H}) - 1.8 \times (\mathrm{J} - \mathrm{K}) \tag{4.1}$$

The selected OB stars are plotted in Figure 4.1 in blue and green. In addition to the stars highlighted in Figure 4.1, we also selected the brightest (e.g 001, 006, 022 & 102) late type stars ($\mathrm{Q_{IR}} > 0.08$) in the field. Another reddening free parameter which is useful in the optical wavelength (see Chapter 5) is given as:

$$\mathrm{Q} = \mathrm{U} - \mathrm{B} - \frac{\mathrm{E(U-B)}}{\mathrm{E(B-V)}}\mathrm{B} - \mathrm{V} \qquad \text{(Johnson \& Morgan 1953)} \tag{4.2}$$

The selected OB targets were used to make a surface density plot (Figure 4.2) to test for clustering (Gomez et al. 1993). A further check on clustering was done using a K vs $J-K$ plot (Figure 4.1 right) which revealed a cluster pattern.

The OB stars in Trumpler 27 field divide themselves into two groups in a K vs $J-K$ plot. There is a group with lower $J-K$ value and another of higher $J-K$. The bright stars in green (maybe SGs) show this clearly (Figure 4.1). The stars we settled on are the ones of lower $J-K$ (demarcated) because they are bluer and their distribution on a K vs $J-K$ plot is more compact. We also included the WC9 star (Gray & Corbally 2009) whose $J-K \sim 3$.

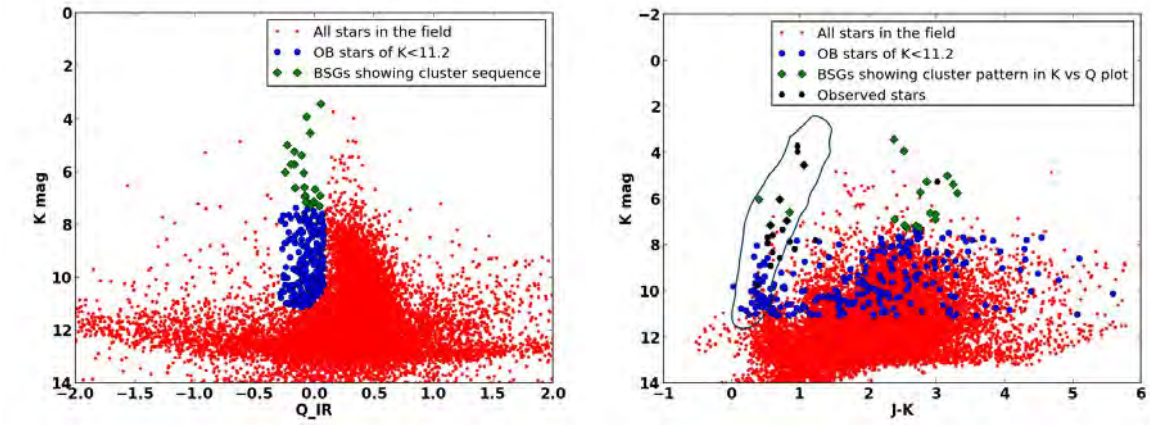

Figure 4.1: Left: K_{mag} vs Q_{IR} diagram for all stars in the field (red), bright early type stars (blue plus green dots). The green points represent possible BSGs Right: K vs $J-K$ plot for all stars in the field (red), bright early type (blue) and the BSGs in green.

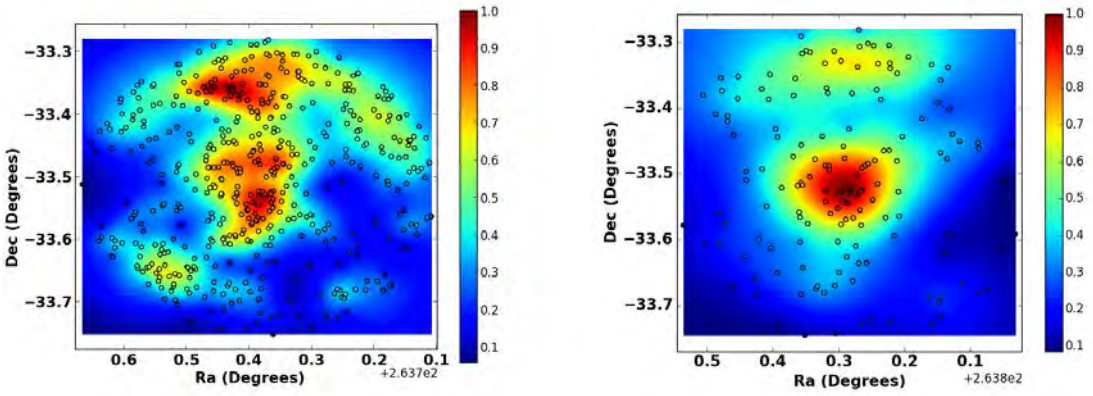

Figure 4.2: Surface density plot of early type stars selected. Right: Early type stars with $\sim 0 < J-K < 1$ on the K vs $J-K$ plot. Red colour correspond to highest density after the densities were normalised (D/D_{max}) with the maximum density in the field.

4.1.1 Selected targets

A total of fifty seven bright stars in Trumpler 27 field were selected for study. The stars comprised early type stars and a few late type stars taken from Moffat et al. (1977). The co-ordinates and K_s magnitude of the selected stars are listed in Table 4.1. The distribution of the stars in this part of the sky is as illustrated on Figure 4.3 with the blue and green squares representing the 19 observed targets while the red circles illustrate non observed objects. The green square represents a Wolf Rayet star in the field.

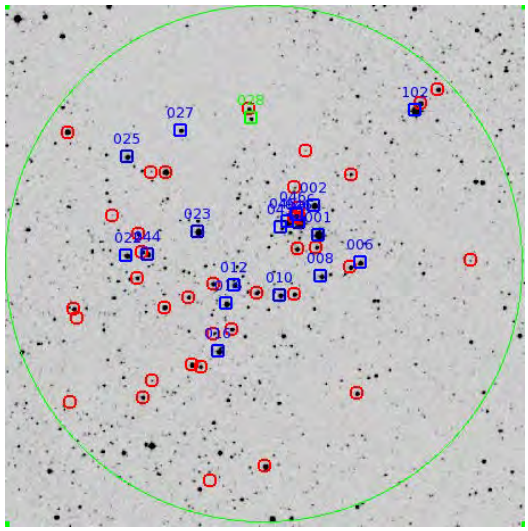

Figure 4.3: A 15′ by 15′ optical image of Trumpler 27 field showing observed stars in blue and green squares. The red circles represent the targets selected but not observed due to time factor. The green circle is the boundary of selected stars.

4.1.2 Data and Observation

Out of the 57 stars in the field selected for spectroscopic observation, only 17 were observed due to time constraints. They were observed in the wavelength range 3800Å to 8900Å using SAAO 1.9m telescope. The observations took place on the nights of 22^{nd} August 2013 to 27^{th} August 2013 using gratings 6, 7 and 10 whose resolutions are $\sim$ 2Å, $\sim$ 5Å and $\sim$ 1Å respectively. The gratings 6, 7 and 10 covered wavelength ranges $\sim$3490Å to $\sim$5423Å, 4243Å to 8143Å and 8316Å to 8934Å respectively.

Five more stars were observed on the nights of 18-24^{th} June 2014 to check on accuracy of the Q method of selection used in the study of earlier stars. The five stars were selected as possible MS members of Trumpler 27 based on their closeness to the MS. Two of the five stars were classified but the rest were discarded due to their low signal to noise ratio (SNR). This put the total number of stars observed and classified in the field to 19.

We also took arc lamps images to assist in calibrating object spectra. We used CuAr arc for gratings 6 & 7 and CuNe arc lamp for grating 10 targets respectively. Biases and

Table 4.1: Co-ordinates and K_s magnitudes (from 2MASS) of the targets. o and n in column 3 show the observed and non-observed respectively.

RA(J2000)	**Dec(J2000)**	**o/n**	K_s **Mag**
17 36 25.49	-33 37 02.45	n	8.23
17 36 33.97	-33 34 02.84	n	3.45
17 36 45.61	-33 34 42.65	n	8.54
17 35 48.37	-33 30 23.75	n	5.01
17 36 09.73	-33 30 54.81	o	6.98
17 36 04.13	-33 30 30.58	o	7.79
17 36 23.35	-33 31 45.29	o	7.93
17 36 24.37	-33 33 10.16	o	7.69
17 36 15.59	-33 31 28.73	o	7.34
17 36 22.17	-33 31 10.74	o	8.32
17 36 37.61	-33 30 18.75	o	8.59
17 36 44.82	-33 32 10.71	n	5.86
17 36 13.65	-33 28 15.69	n	8.92
17 36 10.78	-33 28 47.90	o	7.16
17 36 12.14	-33 27 08.63	n	7.99
17 36 29.95	-33 26 34.28	o	7.87
17 36 27.40	-33 29 35.86	o	6.03
17 36 39.77	-33 29 07.50	n	8.07
17 36 37.62	-33 27 22.17	o	7.59
17 36 34.24	-33 27 49.17	n	7.81
17 35 56.36	-33 25 56.53	n	3.73
17 36 19.91	-33 26 12.43	o	5.27
17 36 12.85	-33 29 19.07	o	3.98
17 36 25.17	-33 32 38.49	n	8.59
17 36 45.18	-33 31 55.27	n	7.95
17 36 45.18	-33 31 55.09	n	7.95
17 36 14.51	-33 29 16.69	o	4.56
17 35 56.36	-33 25 56.53	o	3.73
17 36 17.68	-33 36 35.42	n	8.85
17 36 13.00	-33 28 51.60	n	8.88
17 36 13.20	-33 30 05.30	n	7.1
17 36 10.48	-33 30 02.40	n	10.48
17 36 05.60	-33 30 37.91	n	9.58
17 36 13.60	-33 31 26.70	n	9.19
17 36 19.02	-33 31 24.90	n	11.22
17 36 25.24	-33 31 08.40	n	11.39
17 36 22.52	-33 32 30.10	n	4.84
17 36 26.99	-33 33 37.80	n	9.96
17 36 28.24	-33 33 34.40	n	10.99
17 36 32.20	-33 31 51.49	n	10.29
17 36 28.75	-33 31 32.70	n	8.16
17 36 35.41	-33 30 12.71	n	9.51
17 36 32.10	-33 27 49.00	n	9.24
17 36 46.20	-33 26 37.91	n	9.82
17 36 20.23	-33 25 55.01	n	10.23
17 36 05.59	-33 27 50.80	n	10.58
17 36 35.25	-33 34 32.70	n	11.52
17 36 36.14	-33 30 58.60	n	9.77
17 36 36.00	-33 29 40.50	n	8.19
17 36 34.51	-33 30 16.91	n	6.61
17 36 15.47	-33 29 28.10	o	8.66
17 36 13.63	-33 29 08.30	n	8.92
17 36 12.89	-33 29 10.20	n	8.76
17 36 13.19	-33 29 04.30	n	11.53
17 35 53.16	-33 25 18.01	n	9.53
17 35 55.70	-33 25 43.40	n	9.37
17 36 04.54	-33 34 24.10	o	8.73

dome flat-fields were also taken. Dome flats were taken to take care of variability in CCD pixel sensitivity. The bias images were subtracted from science images to eliminate pedestal levels added to the electron counts in pixels during analogue-to-digital readout process.

Data reduction was done using NOAO IRAF (Image reduction and analysis facility) software *. Biases were averaged and then subtracted from the science data using the tasks `imarith`. Flat-fields were combined using task `imcombine` by taking the median pixel values of the flats. The combined flat was then block-averaged from an image of 88 rows by 1745 columns to 1 row by 1745 columns using task `blkavg`. This task adds row values of a given column and then divide by the number of the rows creating a single average row. The task `blkrep` was later used to replicate the image to its original dimension by spreading the average column value to the original rows. A master flat was then made which was used to divide the target data. Sky subtraction, trace extraction and wavelength calibration were also done using the tasks `apex`, `apall` and `identify` respectively in order to come up with a final wavelength calibrated spectrum.

4.2 Radial velocity

Heliocentric radial velocities (RV) of some grating 10 spectra were estimated using IRAF task `fxcor` of the package `rv`. The spectrum of a RV standard (template) and that of an object were cross-correlated in order to estimate the RV of the object. Radial velocities quoted in most literature are local standard of rest (LSR) radial velocities. We therefore converted the heliocentric RVs from IRAF to LSR for comparison purposes using the formula (www.atnf.csiro.au/people/Tobias.Westmeier/tools_hihelpers.php):

$$V_{LSR} = V_{Helio} + 9\cos(l)\cos(b) + 12\sin(l)\cos(b) + 7\sin(b) \tag{4.3}$$

where l and b are the Galactic longitude and latitude respectively and the velocities are in km/s.

RVs of OB stars have large error bars due to poor spectral match between their spectra and that of template used (G9III star). Similarly, OB stars have fewer lines and there are not many RV standards in the blue thereby complicating cross-correlation. The poor spectral match results in a wide cross-correlation function (CCF).

The height of the peak in the CCF (normally given as height on a scale of 0 -1 on `fxcor`) relative to the rest of the CCF, gives an indication of our confidence in the cross correlation (Alpaslan 2009). Tonry & Davis (1979) suggests that a height that is ≥ 0.5 is good.

An illustration showing a template and an objects spectra is shown in Figure 4.5. The spectra have deepest lines (Ca II) within the regions shown in dotted lines. The object spectrum shown is likely to be for a double star given that each of the Ca II lines seem to have a weaker line on its right side. Such a case also affects the quality of CCF.

*IRAF weblink is http://iraf.noao.edu/

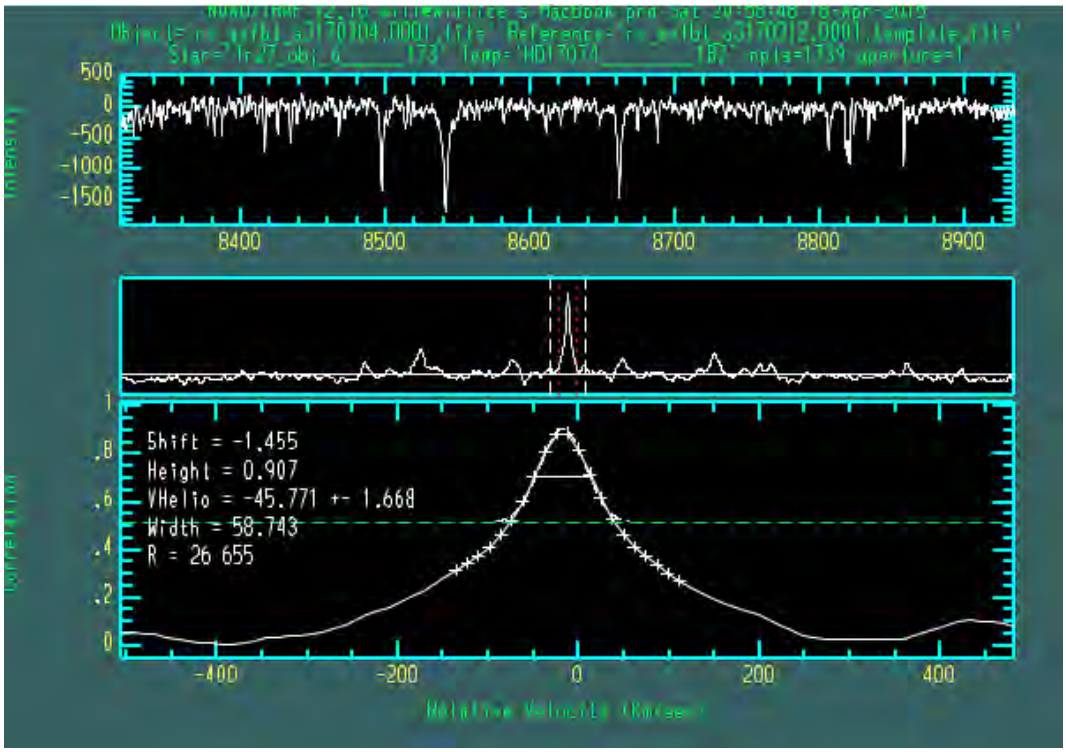

Figure 4.4: Summary of result obtained after cross-correlation. The upper part show object spectrum, middle part CCF and the lower curve is a Gaussian fit on the CCF. Summary of result is also shown on the lower part.

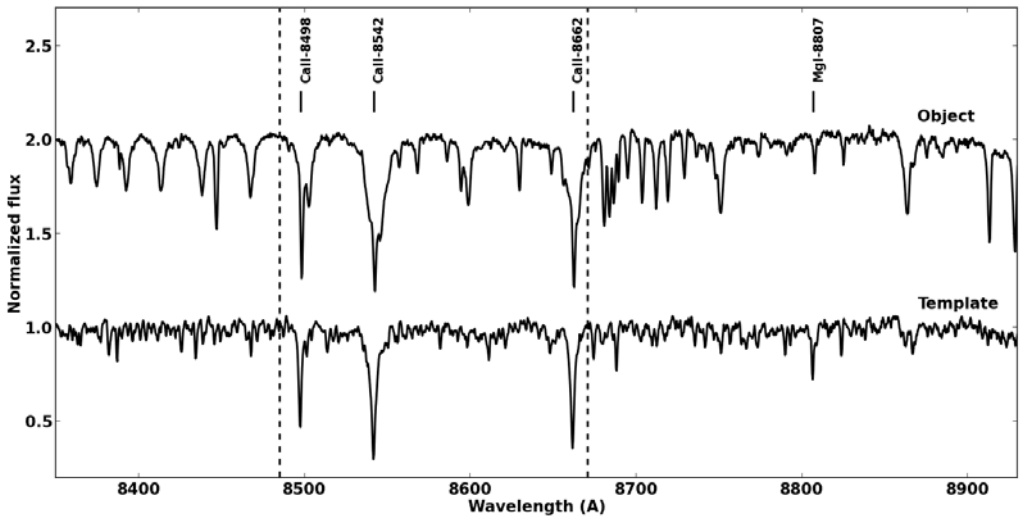

Figure 4.5: Figure showing a radial velocity standard spectrum and that of an object being cross correlated.

4.2.1 Estimating radial velocity of Trumpler 27

Heliocentric RVs of the stars observed in grating 10 were estimated by cross-correlating spectrum of standard star, HD170174 with those of objects. HD170174 is a G9III (Keenan & McNeil 1989) star whose radial velocity is -22.0 km/s (Wallerstein et al. 1963). Kharchenko et al. 2007 and Nidever et al. 2002 estimated the RV of HD170174 as -29.10 ± 0.1 km/s and -28.8 km/s respectively.

Three stars showed good spectral match during cross correlation and their RVs are tabulated in Table 4.2. Two stars (001 & 102) have LSR radial velocities that are consistent with that of Trumpler 27 i.e -15.8 km/s (Kharchenko et al. 2007), -17.34 ± 0.3 km/s (Mermilliod et al. 2008) and -17 km/s (Verheyen et al. 2012). This means that they are likely members of the cluster. Imhoff & Keenan (1976) estimated the RV of 001 which is one of the stars of Trumpler 27 as -11.4 ± 0.7 km/s. It is not clear from Imhoff & Keenan (1976) if -11.4 km/s is heliocentric or Galactocentric RV but it is most likely heliocentric given its closeness to our $V_h \sim$ -12 km/s.

The average radial velocities (LSR) of the two stars is -18.5 ± 2.3km/s, which is our derived RV for the cluster. 006 is an obvious non member given that its RV (∼ -46 km/s) is quite different from that of Trumpler 27. The distance to the cluster can be estimated using equation 4.4 assuming that the cluster participates in Galactic rotation, which is expected of young clusters like Trumpler 27. This method does not give an accurate distance since the derivation of the formula assumes that both the Sun and the cluster are travelling on circular orbits about the Galactic centre which is not true. The derivation of the formula used also assumes that the Galaxy's gravitational potential is axisymmetric and is always directed towards the centre of the Galaxy which ignores the effects of spiral arms and the Galaxy's bar.

$$V_r = Ad\sin(2l) \tag{4.4}$$

V_r is heliocentric radial velocity, d is the object distance and $A \sim 14.8 \pm 0.8$ is Oort's constant (Huyan et al. 2015). The radial velocities of stars 001, 102 and cluster places them at $\sim 4.7 \pm 2$kpc, 1.9 ± 0.8 kpc and 3.3 ± 2kpc respectively.

Table 4.2: Table showing heliocentric radial velocities for some of the stars observed.

Moffat No	**Vh (km/s)**	**LSR (km/s)**	**Cross correlation %**
006	-46 ±2	-55 ±2	91
102	-5 ±2	-15 ±2	75
001	-12 ±5	-22 ±5	78

4.3 Spectral classification of stars

The classification of stars was done by comparing observed spectra with spectral atlases. The atlases used include those from Andrillat et al. (1995) for the near-IR wavelength (∼

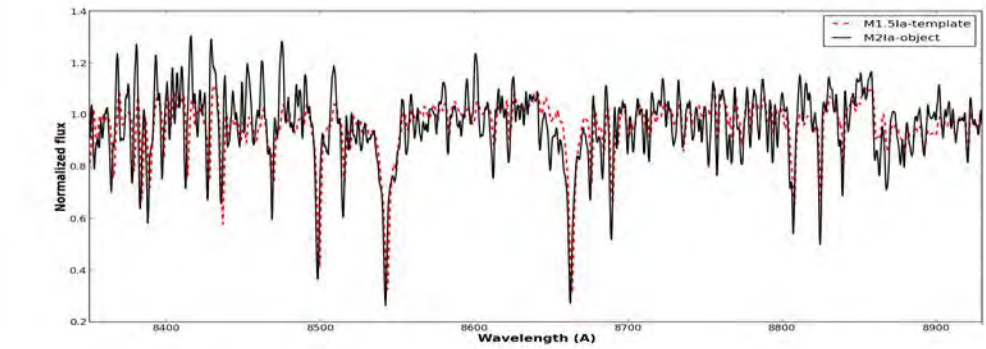

Figure 4.6: Figure showing one of the CATRIPLET templates and an object over plotted to identify the spectral class of the object.

8000Å to 9000Å) and Gray & Corbally (2009) or Walborn & Fitzpatrick (1990) for the blue part of the optical wavelength ($\sim$ 3800Å to 5000Å).

Apart from the spectral atlases we also used Catriplet (Empirical Calibration of the Near-IR Ca II Triplet) * templates. We over-plotted template spectra with that of an object until the best match obtained (Cenarro et al. 2001). An example of a Catriplet template and star spectrum over-plotted is shown in Figure 4.6.

4.3.1 Spectral classes of observed stars.

Spectroscopic results for the 19 observed stars are summarised in Table 4.3. The table shows their spectral classes according to Moffat et al. (1977), Massey et al. (2001) and my work. The star numbers used are as from Moffat et al. (1977). Classification of the early type stars was done using Walborn & Fitzpatrick (1990) and Gray & Corbally (2009) spectral atlases while late type ones were classified using Andrillat et al. (1995) and Kirkpatrick et al. (1991) atlases. CATRIPLET templates were also used to fine tune classification of the late type stars.

Our classification of the late type stars (001, 006 & 102) was based in the wavelength range 8000Å to 9000Å. The spectral results in this wavelength range are inconsistent with those in Massey et al. (2001) who used wavelength range 3750Å - 5000Å. The accuracy in the spectral and luminosity classes are estimated to be one spectral sub-type and one luminosity class respectively.

Star 102 (HD159378) shows the greatest difference in spectral type and is a likely variable supergiant (Van Genderen & Thé 1978) or a binary star with a bluer companion (Van Genderen 1980). The binary case is supported by its spectrum given the weaker lines seen on the right side of the CaII triplets (figure 4.5). Kipper (2008) estimated the effective temperature and spectral class of this star as $T_{eff} = 7500K$ and F0Ia respectively which is closer to our spectral class (F2Ia). This star has been variedly classified from G3Ia to F0Ia and it is likely that the star is changing or the effect of its companion on its spectrum is

*Catriplet weblink is http://pendientedemigracion.ucm.es/info/Astrof/ellipt/CATRIPLET.html

getting stronger.

Table 4.3: Table showing co-ordinates and spectral classes of observed stars. The m or n in the brackets denotes cluster membership and non membership according to Moffat et al. 1977. The spectral classes adopted by Moffat et al. (1977) and Massey et al. (2001) are also given to compare this work with theirs.

Moffat No	RA	Dec	Class	Massey et al. 2001	Moffat et al. 1977
008(m)	17 36 09.73	-33 30 54.81	B0Ia	-	OB
006(n)	17 36 04.13	-33 30 30.58	K2II-III	-	K5III
014 (m)	17 36 23.35	-33 31 45.29	B0Ia	B0Ib	B0Ib
016 (m)	17 36 24.37	-33 33 10.16	B1Ib	B0.5Ia	O9.5II
010 (m)	17 36 15.59	-33 31 28.73	B1V	-	-
012 (m)	17 36 22.17	-33 31 10.74	O9.7Ia	-	OB
022 (n)	17 36 37.61	-33 30 18.75	G5III	-	-
002 (m)	17 36 10.78	-33 28 47.90	B0Ia	B0Ia	O9Ia
027 (m)	17 36 29.95	-33 26 34.28	O8IIf	O8IIIf	-
023 (m)	17 36 27.40	-33 29 35.86	B1Ia	B0.7Ia	B0.5Ib
025 (m)	17 36 37.62	-33 27 22.17	O9V	-	OB
028 (m)	17 36 19.91	-33 26 12.43	WC9	WC9	WN5
046 (m)	17 36 12.85	-33 29 19.07	B8Ia	B8Ia	B9Ia
046a(m)	17 36 14.51	-33 29 16.69	B8Ia	-	-
102(m)	17 35 56.36	-33 25 56.53	F2Ia	G0I	G0Ia
043 (m)	17 36 15.47	-33 29 28.10	B9Ia	B8I	B9Ia
001(m)	17 36 10.07	-33 29 40.26	M2Ia	M0Ia	M0Ia
044(m)	17 36 34.52	-33 30 16.90	B1.5 II-III	B1.5Ia	B1II
046c(m)	17 36 13.21	-33 29 04.50	B0V	-	-

4.3.2 Spectra of stars.

The spectra of observed stars are shown in Figures 4.7 to 4.10.

OB stars

Presence of ionised Helium (HeII-4200 & 4686) lines in a spectrum is an indicator that the star is of spectral type O. HeII-4541 show a decrease in strength from earlier O to later ones. The ratio HeI-4471/ HeII-4541 show a good trend in O stars (Jaschek & Jaschek 1987, Walborn & Fitzpatrick 1990) with HeI-4471 showing an increase and HeII-4541 a decrease from earlier O to later ones. The ratio is ~ 1 in O7 stars. Other lines used in classifying O stars are SiIV-4089 & CIII-(4068, 4647 and 4651) in absorption and N-IIII (4634, 4640) in emission. The ratio HeII-4541/SiIII-4552 which is ~ 1 in O9.7 spectra was used in classifying 012. The NIII emission lines at 4634-4642 and the weaker HeII 4686 are good indicators that star 027 is an O8IIf. The HeII 4686 absorption line is stronger than the emission lines in dwarfs but weaker or comparable in bright giants.

SiIV-4089 & 4116 were used in luminosity classification. They show a decrease in strength as one moves from O supergiants to dwarfs. Dwarfs have broader lines compared to SGs e.g HeII-4541& HeI-4471 clearly show this in O9V. HeII-4686 which is strongest in dwarfs and weakest in supergiants can also be used in identifying luminosity classes.

In OB stars HeI-4471 & MgII-4481 lines show a decreasing and an increasing trend

respectively as one moves from early B stars to later ones. MgII-4481 is minimum at O9 and increases uniformly to $\sim$ A1 where its strength is maximum while HeI-4471 is maximum at $\sim$ O9 and minimum at $\sim$ A0. The ratio HeI-4471/MgII-4481 is $\sim$ 1 at B7. Si IV - 4081/Si III - 4552 which is $\sim$ 1 for B0.7 is a good estimator of B0 - B1 stars. The presence of HeI 4471 & 4861 in B stars confirm their spectral classes since B stars are characterised by strong Balmer and HeI lines. The absence (or very weak) of HeII lines confirm this.

Line widths were used to distinguish between dwarfs and SGs e.g. the lines HeII+H-4861, HeI-4471+MgII-4481 & those of HI in 010 are broader than for other stars (Figure 4.7). Luminosity classification also varies with spectral classes. For example in a B5 star, NII-3995 and Si III triplet at $\lambda \sim 4552$ are used to identify the luminosity classes in the spectral sub class. The lines are stronger in B5Ia stars compared to B5V stars.

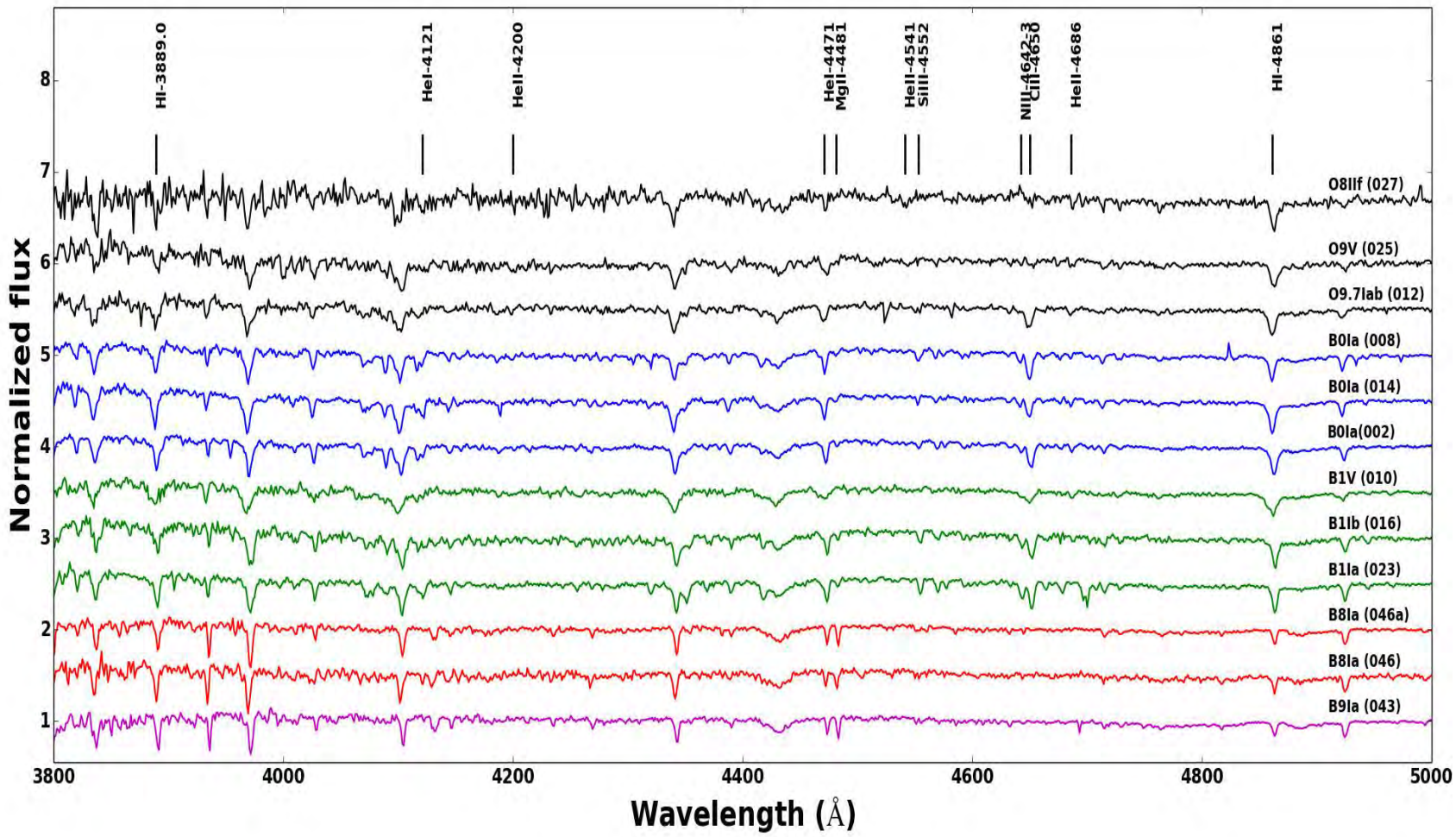

Figure 4.7: Observed OB stars' spectra in the wavelength range 3900-5000Å.

Wolf Rayet (WR) Star spectrum:

The WR95 (also known as He3-1434) spectra shown (Figure 4.8 and 4.9) are characterised by strong emission lines due to their strong and powerful winds (Jaschek & Jaschek 1987). These stars are hot, given the presence of HeII lines e.g at λ =4686Å expected in hot (∼30000-60000K) stars. The spectrum of 028 closely matches a WC9 WR template from Gray & Corbally (2009) indicating that WR95 is a WC9 star.

The ratio CIV-5808/CIII-5696 is < 0.4 (Gray & Corbally 2009) and CIII-4650/HeII-4686 > 0.8 confirming the classification. The HeII-4686 line is only clear in WC9 spectra. Massey et al. (2001) and van der Hucht (2001) classified the star as WC9 and WC9d respectively which are in agreement to our adopted class. Another spectrum of 028 in the wavelength range 5000Å to 7000Å is also shown in figure 4.9.

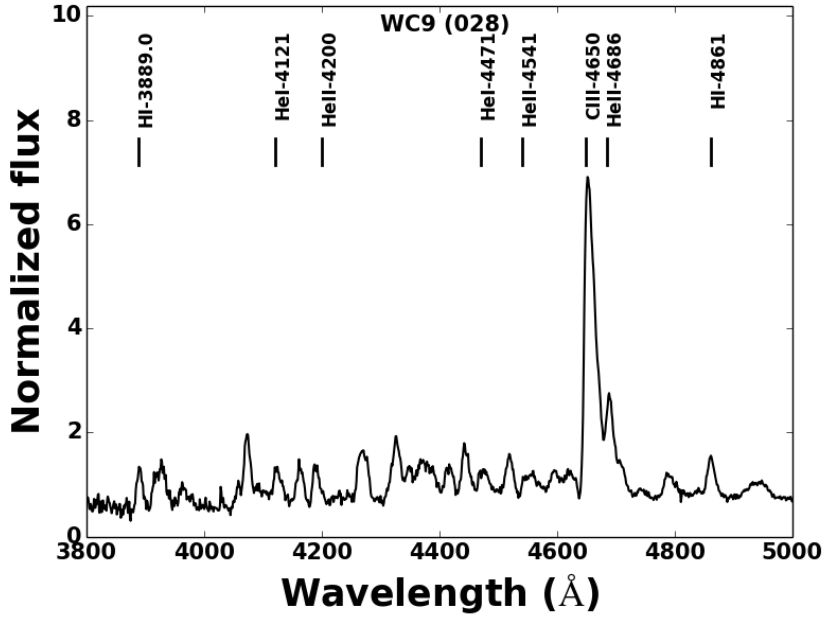

Figure 4.8: Wolf Rayet star (028) spectrum in the wavelength range 3800Å to 5000Å.

Wavelength range 8000Å-9000Å:

Classification of the stars was done by identifying the changes in CaII triplets (8542Å, 8662Å and 8498Å), TiO band, the Paschen lines among other features (Andrillat et al. 1995) as shown inn figure 4.5. CaII triplets are strongest in late K through to mid M stars (Kirkpatrick et al. 1991). The CaII lines and FeI-(8757 & 8764Å) are strongest in SGs and giants but weaker in dwarfs. FeI-8440, which is obvious in K and early M stars, confirmed that 006 and 001 are K and early M stars respectively. Figure 4.10 shows spectra of three stars spectroscopically observed.

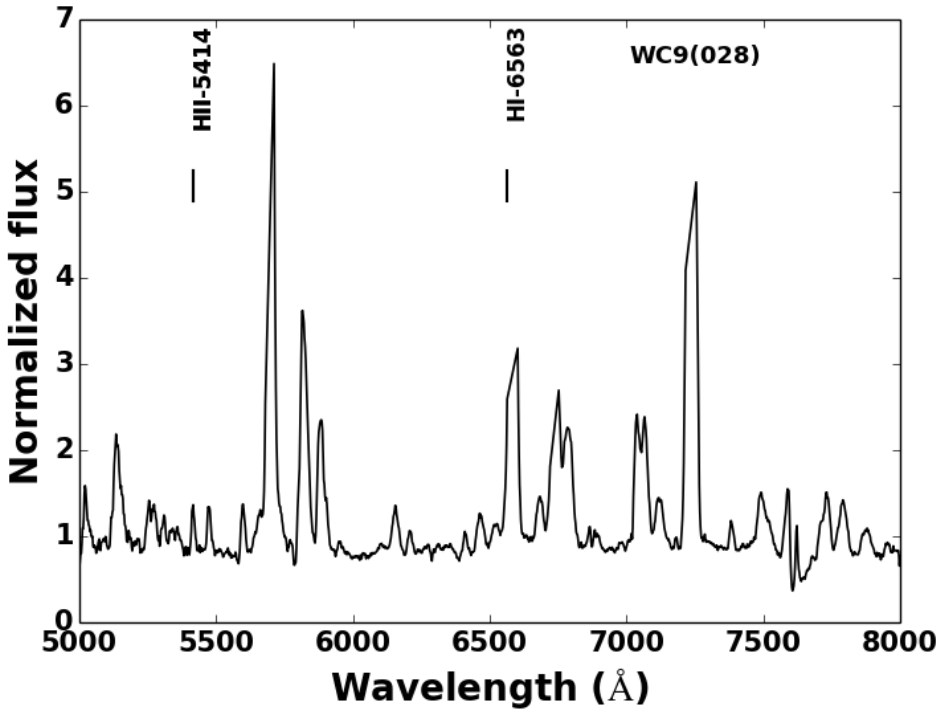

Figure 4.9: Spectrum of Wolf Rayet star 028 from 5000Å to 8000Å

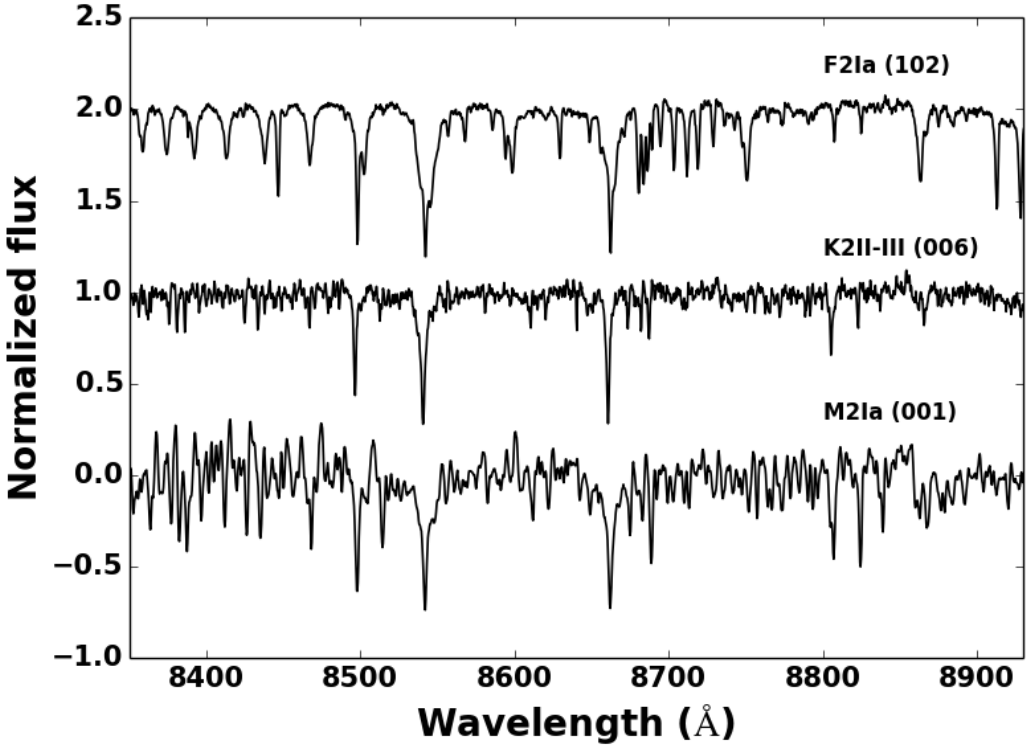

Figure 4.10: Spectra of the late type stars (001, 006 & 102) observed.

Chapter 5

Photometric analysis of Trumpler 27

5.1 Analysis of observed stars

Properties of stars such as temperature, age and brightness can be inferred from their spectral classes. Table 5.1 lists some of the quantities that were derived from spectral classes of the observed stars. The intrinsic colours $(B-V)_o$ and absolute magnitudes (M_V) of the stars shown on table 5.1 were read from Fitzgerald (1970) and Gray & Corbally (2009) respectively based on spectral classes of the stars. $(B-V)_o$ and M_V values of the stars were used to estimate their ages, initial masses (M_{in}) and current masses (M) from Ekstrom et al. (2012) isochrones. An error of one spectral subtype or one luminosity class as estimated in the classification of the stars results in an average $(B-V)_o$ and M_V errors of ~ 0.02 and 0.7 respectively. The M_V errors are higher in dwarfs compared to supergiants. An error of ~ 1.0 in M_V results in an age error of about $\sim 4-6$ Myrs at $\sim 10^7$ years.

The ages of the dwarf OB stars are in the range of $\sim 10^{6.7}-10^{7.1}$ years while the ones of supergiants lie between $\sim 10^{6.6}$ and $\sim 10^{7.0}$years. The later OB supergiants are older than the earlier ones by ~ 6 million years which is within the error stated earlier meaning that all the stars belong to a single population. The F2 and M2 supergiants are approximated to be $\sim 10^{6.9}$ and $\sim 10^{7.0}$ years old respectively which are in agreement with some OB dwarf and supergiant ages.

The ages of most observed stars lie between $10^{6.6}-10^{7.1}$ years except 006 and 022 which are obvious non members. 006 is too old while 022's is too young to fit the age bracket of the other stars of the cluster. 006's radial velocity also confirm that it is not a member of the cluster. The stars' ages divide them into two groups, older ones (age range $\sim 10^{6.9-7.1}$) with an average age of $\sim 10^{7.0}$ and younger ones. The older group contains the cool supergiants, two early type dwarfs (010 and 046c) and four BSGs (016, 046, 046a, 043). The younger group (average age $= 10^{6.63}$) is made up of WC9, O stars and B stars earlier than B2. Figure

Table 5.1: Table showing Moffat et al. (1977) numbering, SpT, $(B-V)_o$, M_V, $Log\ Age$, M_{in} and M of the observed stars.

Moffat No	SpT	$(B-V)_0$	M_V	$\sim \log\ Age \pm 0.2$	M_{in}	M
008(m)	B0Ia	-0.24	-7.0	6.60	45.31	40.44
006(n)	K2II-III	1.15	-1.4	8.10	4.56	4.55
014(m)	B0Ia	-0.24	-7.0	6.60	45.31	40.44
016(m)	B1Ib	-0.19	-5.7	7.00	16.58	16.35
010(m)	B1V	-0.26	-3.5	7.10	12.50	12.44
012(m)	O9.7Ia	-0.27	-7.0	6.60	52.86	19.05
022(n)	G5III	0.9	0.4	5.25	4.43414	4.4341
002(m)	B0Ia	-0.24	-7.0	6.60	45.31	40.44
027(m)	O8IIf	-0.30	-5.9	6.70	29.93	28.53
023(m)	B1Ia	-0.19	-7.0	6.70	36.83	14.25
025(m)	O9V	-0.31	-4.3	6.70	18.24	18.13
028(m)	WC9	-0.456	-4.97	6.50	104.86	25.4
046(m)	B8Ia	-0.01	-7.1	7.00	16.77	16.34
046a(m)	B8Ia	-0.01	-7.1	7.00	16.77	16.34
102(m)	F2Ia	0.18	-8.4	6.90	20.39	18.42
043(m)	B9Ia	0.00	-7.1	7.00	16.80	16.33
001(m)	M2Ia	1.65	-7.0	7.00	12.99	12.02
044(m)	B1.5II-III	-0.27	-4.7	7.00	16.56	16.633
046c(m)	B0V	-0.30	-4.1	6.90	17.03	16.85

5.1 is an illustration showing the stars and their approximate ages.

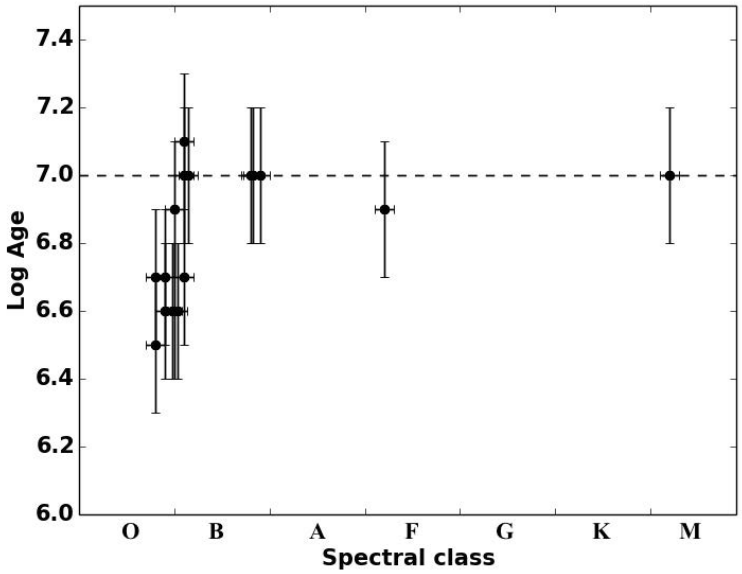

Figure 5.1: Age vs spectral type of observed stars.

Ekstrom et al. (2012) isochrones were fit into M_V vs $(B-V)_o$ plot of spectroscopically observed stars to find out if they evolve as a group (coeval). The stars identified as non members (006 & 022) were not used in the fit.

The age of the cluster was constrained using the cool supergiants that fit an isochrone of $10^{6.9}$ years quite well since the early type stars' ages spread a lot from $\sim 10^{6.6}$ to $10^{7.2}$ years. The spread in age of the early type stars can be attributed to errors in spectral and luminosity classification which has effect on a star's M_V. A change in a star's M_V results in a change in its age.

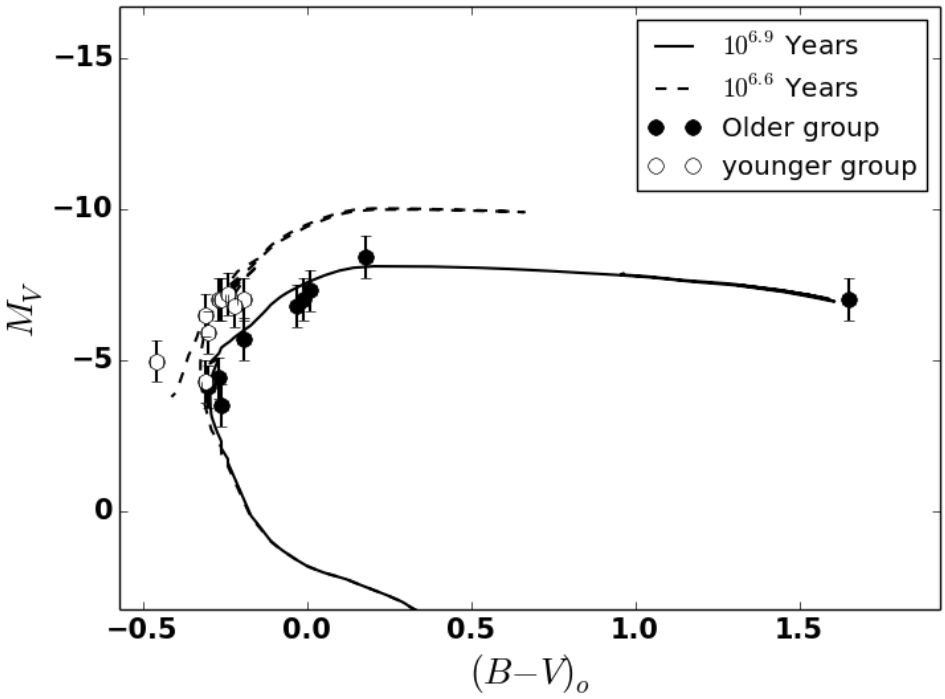

Figure 5.2: Isochrone fits into observed stars.

Massive stars in a cluster have been found to trigger formation of more stars in the periphery of a HII region that harbour them. The secondary stars' formation is due to primary stars' high radiation pressure (Deharveng et al. 2008) which compress gas in the HII region thereby aiding formation. The age gap can therefore be the time between the formation of first generation stars and the second generation ones whose formation were triggered by the older massive stars in the cluster. Apart from 002 which is at the core of the cluster and 008 which is close to the core, all the other stars appear to be at the periphery of the core. The location of the younger stars support the idea that they were formed later than the core.

Distance to the Observed stars

When the observed stars are de-reddened assuming standard extinction law (see Table 5.2) and their CMD made, they all fit a $10^{6.9}$ years isochrone irrespective of their age differences noted earlier. This can be attributed to large dipersions in absolute magnitude calibration where a small mistake in luminosity class (i.e. Iab instead of Ib) result in quite a different values of M_V. Also, it is clear that different authors (Gray & Corbally 2009, Wegner 2006 & Ekstrom et al. 2011) do not agree on theoretical values of M_V.

The distance to the stars can be estimated by fitting a MS to the main sequence stars (025, 010 & 046c) in their CMD. The distance to the MS stars was estimated as $\sim$ 1.4 kpc and $\sim$ 3.6kpc for (025 & 010) and 046c respectively. This is because a MS fit into (025 and 010) resulted in a distance modulus of 10.8 while 046c's DM is 12.8 as shown in Figure 5.3. A more accurate estimate of the distance is given in the next section using more stars from photometric data.

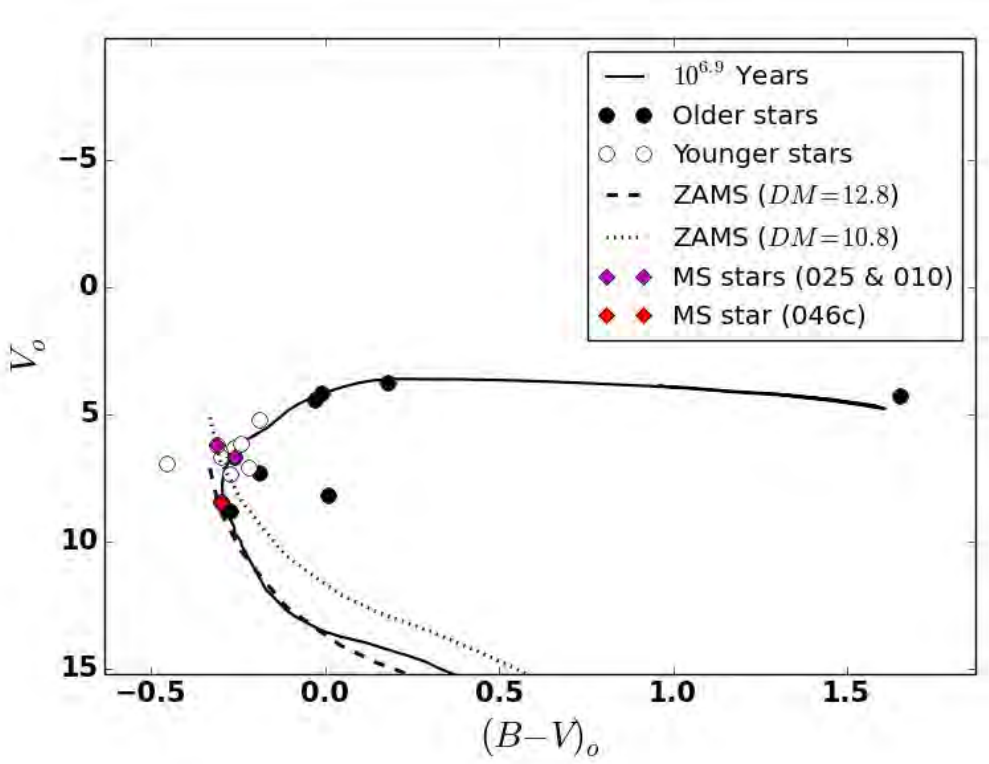

Figure 5.3: Dereddened CMD showing the position of observed stars and isochrone of age $10^{6.9}$ (Ekstrom et al. 2011) and the ZAMS at two different distances of 1.3 and 3.6 kpc

5.2 Analysis of stars in Trumpler 27 field.

To make a more informed decision about the cluster, all stars in Trumpler 27 field were analysed based on Perren et al. (2012)'s deep CCD photometric data. The data is made up of $\sim$ 9000 stars out of which 2000 have all their V, $B-V$, $U-B$ and $V-I$ values and are the ones used in analysis. Their mean errors are: 0.036, 0.048, 0.030 and 0.039 for $U-B$, $B-V$, V and $V-I$ respectively which are slightly larger than the one spectral sub-class($B-V \sim 0.02$) estimate. Moffat et al. (1977) also did photometric study of the field using a combination of photoelectric and photographic data.

The two sets of data show a few differences between them, as the average deviations between Perren et al. (2012) and Moffat et al. (1977) data are only $\Delta V = -0.08 \pm 0.15$, $\Delta(B-V) = -0.19 \pm 0.15$ and $\Delta(U-B) = -0.23 \pm 0.17$ (Perren et al. 2012). Photometric data from Perren et al. (2012) for our spectroscopically observed stars are tabulated on table 5.2.

The intrinsic colour indices $(B-V)_0$ & $(B-U)_0$ of the observed stars listed on the table were read from Fitzgerald (1970) based on their spectral classes while the de-reddened visual magnitudes V_o were estimated using the standard extinction law $V_o = V - 3.1 \times E(B-V)$. Where V is the apparent visual magnitude and $E(B-V)$ is the colour excess.

Table 5.2: Table showing Moffat et al. (1977) numbering, V, $B-V$, $U-B$, $(B-V)_0$, $(U-B)_0$, $E(B-V)$ and V_o of the observed stars.

Moffat No	V	$B-V$	$U-B$	$(B-V)_0$	$(U-B)_0$	$E(B-V)$	V_o
008(m)	11.693	1.552	0.268	-0.24	-1.01	1.792	6.14
006(n)	11.521	1.203	1.136	1.15	1.06	0.053	11.36
014(m)	11.099	1.086	-0.003	-0.24	-1.01	1.326	7.05
016(m)	10.723	0.926	-0.125	-0.19	-0.99	1.116	7.26
010(m)	11.890	1.425	0.264	-0.26	-0.95	1.685	6.67
012(m)	12.032	1.246	0.124	-0.27	-1.08	1.516	7.33
022(n)	11.373	1.028	0.670	0.9	0.21	0.128	10.98
002(m)	10.503	1.096	0.011	-0.24	-1.01	1.336	6.30
027(m)	13.103	1.786	0.423	-0.30	-1.14	2.096	6.64
023(m)	09.999	1.365	0.106	-0.19	-1.01	1.555	5.18
025(m)	11.314	1.343	0.149	-0.31	-1.13	1.653	6.19
028(m)	13.136	1.553	0.345	-0.456		2.009	6.91
046(m)	08.691	1.463	0.251	-0.01	-0.64	1.473	4.12
046a(m	10.129	1.812	0.437	-0.01	-0.64	1.822	4.42
102(m)	08.437	1.699	1.246	0.18	0.24	1.519	3.73
043(m)	13.618	1.767	0.495	0.00	-0.60	1.677	8.42
001(m)	08.479	3.017	0.072	1.65	1.69	1.367	4.24
044(m)	12.088	0.791	-0.252	-0.27	-0.95	1.061	8.80
046c(m)	13.260	1.255	0.110	-0.30	-1.08	1.555	8.44

Reddening / Extinction law to Trumpler 27 field.

$E(B-V)$ of the stars are greater than one except for 006 and 022 (Table 5.2). These two stars are foreground stars as noted by Moffat et al. (1977) and were therefore not used in estimating reddening law to Trumpler 27 field. The cool SGs spectroscopically observed were also not used in estimating reddening law since their intrinsic colours are not well constrained (Fitzgerald 1970) given their rare number.

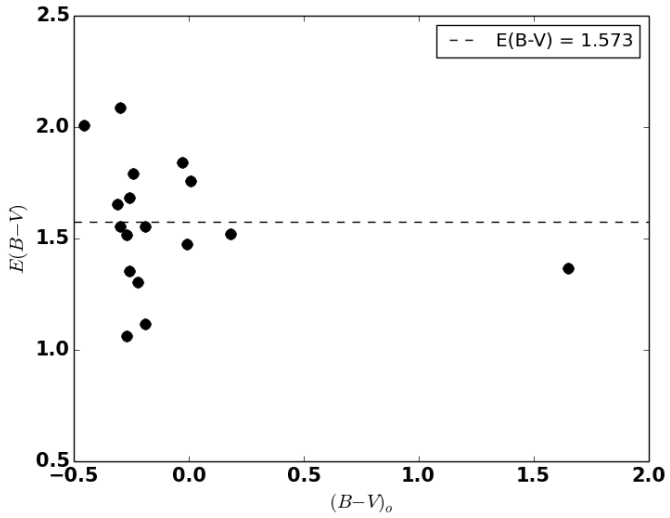

Figure 5.4: Variation of colour excess E(B-V) with intrinsic colour of observed stars.

Figure 5.4 of colour excess versus intrinsic colour reveal that the stars are variably reddened since stars of same spectral class (intrinsic colour) have different reddenings. The figure also show that the effect of variable reddening is higher in earlier type stars compared to later type ones (even in B stars alone). This may be the reason for the wide magnitude spread between the MS stars used in estimating distance of the observed stars (see table 5.2). The average reddening of the stars excluding 006 & 022 is $\sim 1.6 \pm 0.3$ putting the distance to the stars at $\sim 2.5 \pm 0.5$ kpc ($d = \frac{A_V}{2}$ for $b \leq 2^o$ (Bradt 2003)). Moffat et al. (1977) estimated the cluster's colour excess to be ~ 1.4. The $E(B-V)$ standard deviation of 0.3 results in a large error in distance of ~ 0.5 kpc showing how a small variation in reddening gives rise to a large change in distance estimate.

The reddening law was estimated from the ratio of colour excess of observed stars $\frac{E(U-B)}{E(B-V)}$. The ratio is 0.73 ± 0.04 for the observed stars as estimated from the gradient of $E(U-B)$ vs $E(B-V)$ plot (Figure 5.5). This ratio is crucial in estimating intrinsic colours of other stars in the field using a reddening free quantity called the Q parameter (see next section). Since the value of the reddening constant (0.73) is close to the standard reddening law (0.72), we opted to use $R_V = 3.1$ (standard extinction) in studying other stars in the field.

Effects of variable reddening on the plot is seen on the scatter of the data points. The

OB stars used are variably reddened that a line of best fit of $E(U-B)$ vs $E(B-V)$ plot has a goodness of fit (R^2) that is only 0.659. Another possible cause of the spread is errors made in spectral classification of the stars. An error of one spectral subtype in early B stars results in an average $E(B-V)$ and $E(U-B)$ error of ~ 0.03 and 0.09 respectively.

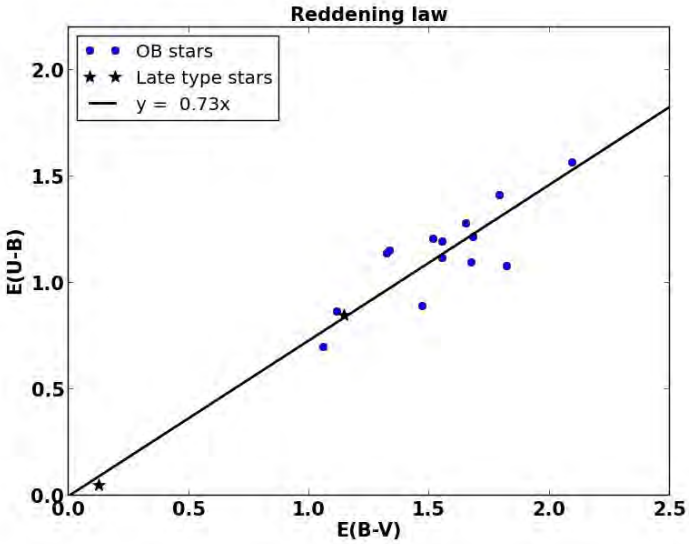

Figure 5.5: Reddening law for the observed OB stars. The reddening ratio is 0.73 $\pm$0.04 with a goodness of fit of $R^2 = 0.659$.

5.2.1 Selection of cluster members

Perren et al. (2012) conducted deep photometry of Trumpler 27 field collecting data for $\sim$ 2000 stars successfully. Some of the stars are not members of the cluster and selection of the cluster members from the data was necessary. To select cluster members, Q parameter was used to identify early type stars in the field since they are young and associated with open clusters. Spatial, MS fit and photometric selection techniques were applied in identifying Trumpler 27 stars from the numerous stars in its field.

Q Spectral typing

A reddening free quantity called $Q-$ parameter is effective in estimating the intrinsic colours of B stars. This is because Q and spectral type of $B0$ to $B9$ stars have a linear relation (Johnson & Morgan 1953) as shown in Figure 5.6. The method of estimating the spectral type and intrinsic colour $(B-V)_o$ of a star from its Q value is called Q spectral typing. $B0$ to $B9$ stars have Q values ranging from ~ 0 for $B9$ stars to ~ -0.9 for $B0$ stars. The parameter is calculated using the formula:

$$Q = (U-B) - \frac{E(U-B)}{E(B-V)}(B-V) \tag{5.1}$$

Q-parameter depends on the ratio of colour excess values $\frac{E(U-B)}{E(B-V)}$, called the reddening law. A standard reddening law has a ratio of 0.72 which can change depending on dust composition.

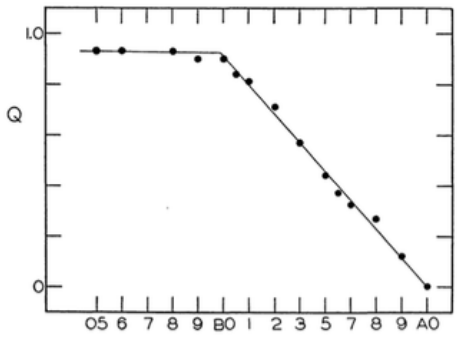

Figure 5.6: Relationship between spectral type and Q of B stars. Linearity is from $B0$ to $B9$ (Johnson & Morgan 1953).

Intrinsic colour indices, $(B-V)_o$, of the stars were estimated from their Q values using the formula (Binney & Merrifield 1998, Gutierrez-Moreno 1975):

$$(B-V)_0 = 0.332 \times Q \tag{5.2}$$

Estimating absolute magnitudes of stars in Trumpler 27 field

The absolute magnitudes of the stars were estimated from their $(B-V)_0$ using linear relationships between $(B-V)_0$ and M_V for un-reddened MS stars (Drilling & Landolt 2000). Four equations were derived from the CMD (Figure 5.7) of the un-reddened MS stars. Equations of $L1$, $L2$, $L3$ and $L4$ were used to estimate the M_Vs within the regions where the lines coincide with the plot. The lines work well for all stars whose $(B-V)_o < 0$ (earlier than A0). The equations used are:

$$L1 : M_V = 60(B-V)_0 + 14.1 \; for \; -0.33 < (B-V)_0 < -0.3 \tag{5.3}$$

$$L2 : M_V = 17(B-V)_0 + 1.65 \; for \; -0.24 < (B-V)_0 < -0.11 \tag{5.4}$$

$$L3 : M_V = 26.83(B-V)_0 + 4 \; for \; -0.3 < (B-V)_0 < -0.24 \tag{5.5}$$

$$L4 : M_V = 9.7(B-V)_0 + 0.85 \; for \; -0.11 < (B-V)_0 < 0.05 \tag{5.6}$$

Selecting MS stars from V/Q plot.

A V/Q plot is an important tool for identifying a cluster in a field where stars are variably reddened (figure 5.8). Some other benefits of the plot are: its use in selecting cluster stars and estimating cluster distance. A main sequence fit in the V/Q plot of Figure 5.8 reveal

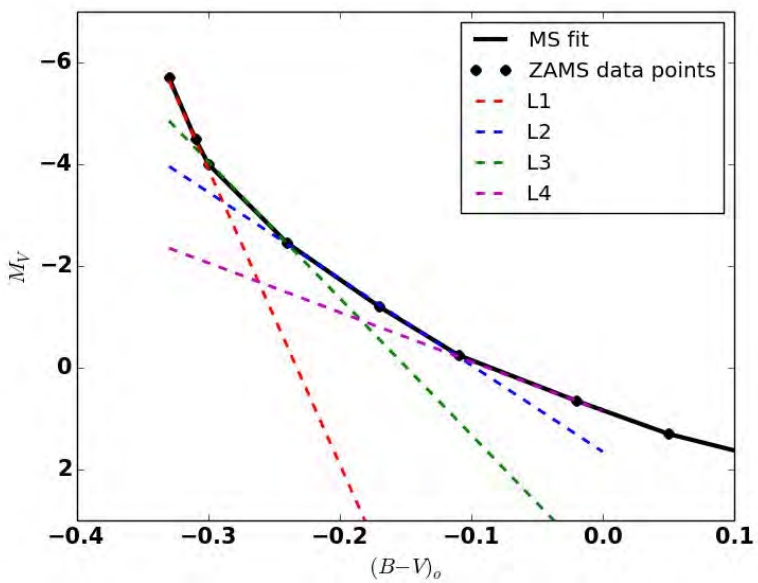

Figure 5.7: Lines used to estimate the M_Vs of stars from their intrinsic colours assuming that they are MS stars (Drilling & Landolt 2000).

that there is a cluster whose MS members lie within the region marked in blue. Blue points that lie within $\sim -0.5 \leq Q \leq -1$ clearly show that there is a cluster in the field.

Stars whose Vs are ~ 1 (to include as many stars as possible) magnitude away from the MS were selected as possible main sequence stars. A total of $\sim$ 1200 stars were selected using the V/Q plot. Some of the stars marked in blue may be non members and more work e.g eliminating late type stars whose Q values are similar to those of early type stars using $(B-V)$ vs Q plot is needed to single out real members. This is addressed in the next section. One challenge in using V/Q plot is that Q parameter does not give information about a star's luminosity.

Eliminating late type and foreground stars using $(B-V)$ vs Q plot.

Open clusters are dominated by OB stars but Q selection allows for inclusion of some late type stars since they have Q values that are similar to those of early type stars (Figure 5.9). Moffat et al. (1977) estimated the ratio of BSGs to RSGs in Trumpler 27 as 6:1 confirming that OB stars dominate this cluster too. To eliminate both late type stars and foreground ones, $B-V$ vs Q plot was used. The late type stars have higher $B-V$ values while the foreground ones are less reddened making it easier to single them out (Figure 5.9). Approximately 100 stars were identified as late type stars whose Q values are similar to those of early type stars and were rejected from the sample.

The plot also reveal that there is differential reddening in the field given that stars of the same spectral class have different apparent colours. The differential reddening complicates

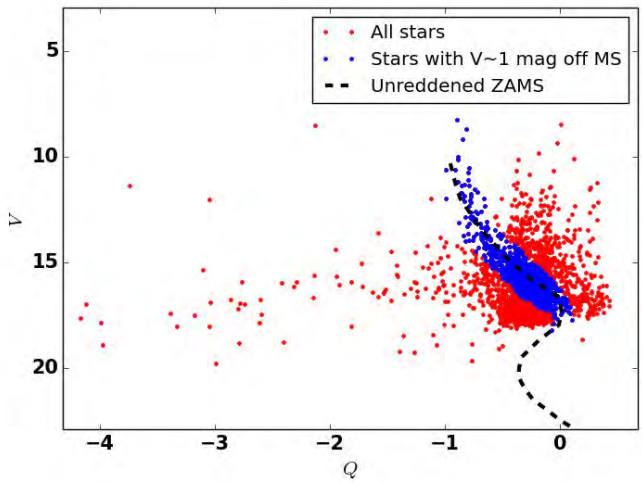

Figure 5.8: V/Q for all stars in the field (in red). Blue points represent possible cluster MS members.

the process of selecting cluster members meaning that some of the stars selected may be non members.

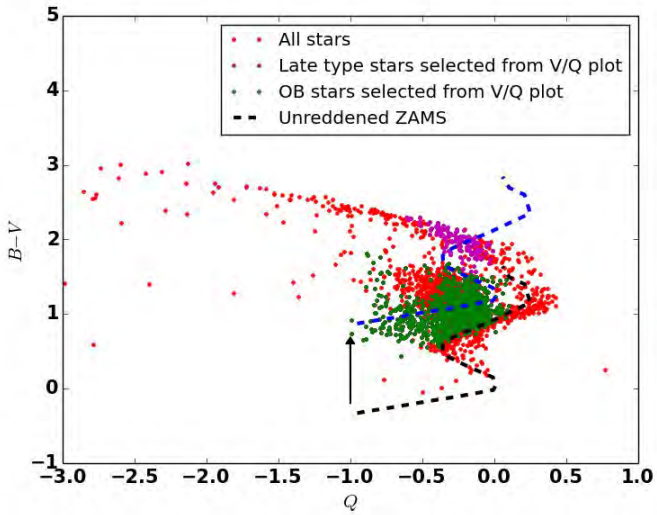

Figure 5.9: Green points represent stars selected using the said procedure. Late type stars from V/Q plot are represented by magenta points. The arrow shows the reddening vector of $E(B-V) = 1.5$. The black and blue dashed lines are unreddened and reddened ZAMS lines respectively.

Identifying cluster members using $V_o - M_V$ vs V_o plot.

Trumpler 27 field is highly and variably reddened therefore identifying its members is not an easy task. A plot of $V_o - M_V$ vs V_o is a powerful tool that can be used to identify members of a cluster in such a field (The & Stokes 1970). Stars in a cluster arrange themselves along an evolutionary deviation curve (Johnson 1960) similar to the one shown in figure (figure 5.10). This is a curve that shows deviation in stars' absolute magnitude δM_V based on their brightness as they evolve. A fit of an evolutionary deviation curve to cluster data points can also be used to estimate a cluster distance.

Figure 5.10 reveals that there are two groups of stars, one to the left and another to the right. Both of them are fit with the evolutionary deviation curve to identify stars that form a cluster. The red points of figure 5.10 show a pattern that is very similar to the deviation curve and are the ones considered as stars of a cluster. The group represented by red points consists of the brightest stars in the field as can be seen from the stars' visual magnitudes meaning that it is the one with supergiants (massive stars). The rest of the points (blue) on the plot represent background stars since they are fainter and older compared to the cluster ones. These points do not form any clear definite pattern. Some stars represented by the blue points may belong to the cluster but it is difficult to separate them especially towards the curves' junction.

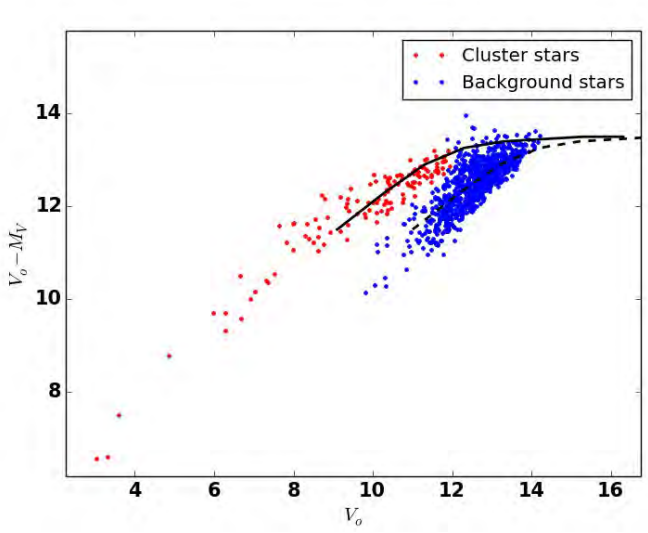

Figure 5.10: $V_o - M_V$ vs V_o plot for early type stars selected from $B - V$ vs Q plot. The stars split themselves into two groups in the plot. The continuous and dotted lines are evolutionary deviation curve fits (Johnson 1960).

Spatial selection of stars

Density plots for stars selected from figure 5.10 were made separately as shown in figure 5.11. The groups show distinct difference with the one on the left showing cluster behaviour with

some interlopers while the one to right having an extended pattern that is not characteristic of a cluster. The plot on the left panel of figure 5.11 is therefore the cluster's. The cluster is centred at $\alpha \sim 264.1$, $\delta \sim -33.5$ and covers an area measuring $\sim 13'$ by $11'$. The cluster has a total of 129 stars most of which are concentrated at the core.

Figures 5.11 reveal that there is a ring-like cloud around the cluster which is a good guide in search of cluster stars. The number density of stars also reduce gradually as one moves away from the cluster centre towards the edge. This is an important indication of cluster presence in a given part of the sky.

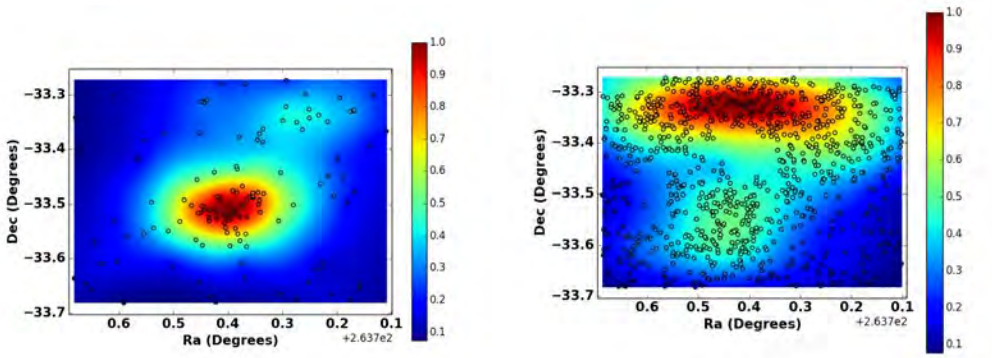

Figure 5.11: Left: Spatial distribution of photometrically selected stars in the field (Red points of figure 5.10). Left: Stars considered to be for a cluster. Right: Stars discarded as field stars (Blue points of figure 5.10).

Refining selection using $V - M_V$ vs $E(B - V)$ plot.

A plot of $V - M_V$ vs $E(B - V)$ is useful in estimating intrinsic extinction constant R_V of a cluster and the distance to the cluster. Figure 5.12 was made using stars whose density plot is given in figure 5.11 left. The plot suggest that there are two populations in the selected stars. These could be either two clusters, a cluster and background stars or another effect of differential reddening causing a lot of scatter in the diagram.

The group represented by blue points (figure 5.12) is a cluster while the red points represent either background stars or another cluster. The cluster is ~ 1.7 kpc away from the sun according to the standard reddening law fit into the least reddened star in the group. This method is not reliable since the least reddened star may have been eliminated during selection of stars.

The background stars spread from a distance of ~ 2.7 kpc to ~ 4.2kpc but have highest density at ~ 3.5 kpc away. Separating the background stars from the cluster is the biggest challenge in studying Trumpler 27 and that is why Perren et al. (2012) suggested that it is not a cluster or that there are two or more clusters that overlap. Figure 5.12 strongly support the idea of a cluster behind Trumpler 27 hence the two clusters along the same cone of sight as proposed by Perren et al. (2012). All the observed stars belong to the blue points

and are marked with diamond in Figure 5.12. Spatial distributions of the groups are shown in Figure 5.13 and support clustering behaviour.

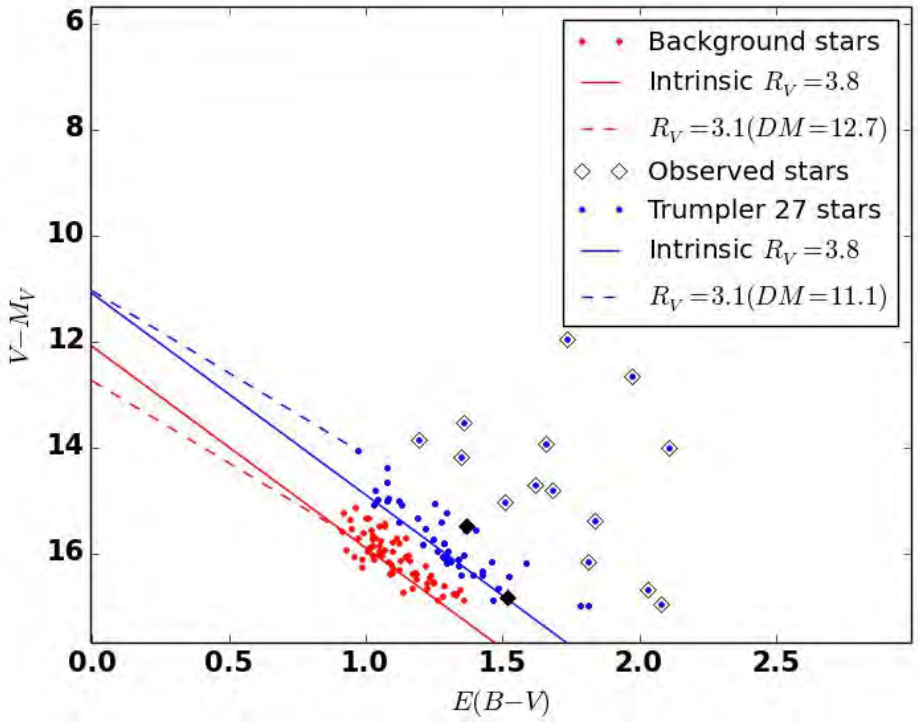

Figure 5.12: Red points illustrate background stars while the blue ones are for the cluster. The continuous lines give intrinsic R_V of 3.8 while the dotted ones are standard extinction law fits on least reddened star of each group. The two black diamonds are the observed cool SGs.

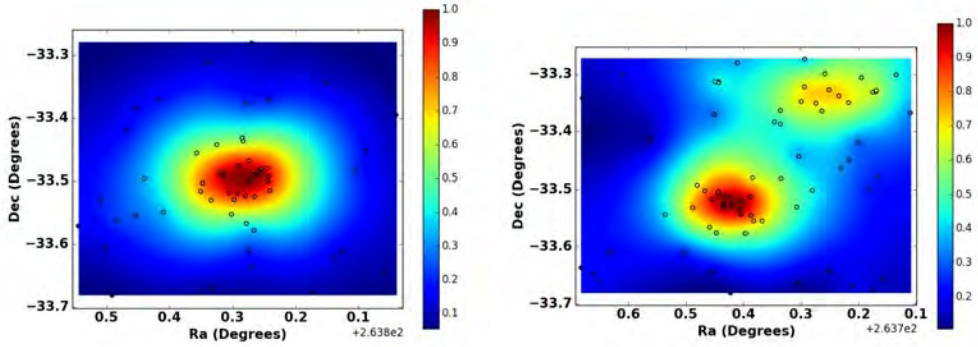

Figure 5.13: Spatial distribution of blue (left) and red (right) points of figure 5.12.

Distance and Age of Trumpler 27

Using the selected MS stars and massive stars observed, we get estimates of the cluster's distance and age as $\sim 2.6 \pm 0.2$ kpc and $\sim 10^{7.0\pm0.2}$ respectively. The distance derived from the CMD agrees well with Massey et al. (2001)'s distance of 2.5±0.3 kpc that they derived from spectroscopic parallax. The errors were estimated from the range in isochrones that bracket our data.

The MS of the stars is wide due to variable reddening which affects earlier stars more (O9 - B1 as noticed in figure 5.4). Since most of the stars selected lie in this category, the MS must be wide.

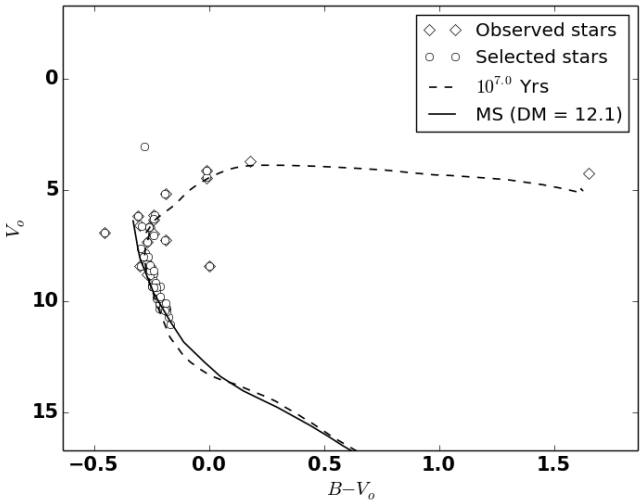

Figure 5.14: MS fit on selected stars giving a DM of 12.10 ($\sim$ 2.6 kpc). The isochrone fits age is $\sim 10^{7.0\pm0.2}$ years.

5.2.2 Cluster membership

Based on the optical and infrared study of the field, a number of stars were considered as the most likely members of Trumpler 27. The stars were selected based on their closeness to the MS and isochrone fits of the CMD (V_o vs $B-V_o$) diagram (figure 5.14). A total of 54 stars were identified. It is not clear if the WC9 star is part of the cluster since the isochrone fit is too old to have a WR star (Ekstrom et al. 2011).

The cool supergiants F2Ia and M2Ia belong to the cluster. This suggestion is supported by their RVs (ours and Mermilliod et al. 2008's), colour excess values and their closeness to the isochrone fit. They are $\sim 5'$ or 3.8 pc apart assuming a cluster distance of 2.6 kpc.

The BSGs spectroscopically observed all appear to belong to the cluster based on their proximity to Isochrone and MS fits used except 043 (B9Ia) that is too faint to be at the same distance with the rest. The luminosities of the BSGs, as derived from the photometry,

vary a lot (from $V_o \sim 4.12$ to 8.42) which is attributed to strong differential reddening. The visual magnitudes of the fainter BSGs also give a strong suggestion that there is a cluster right behind Trumpler 27 made up of the faint BSGs and some of the background stars (Figure 5.12).

A list of 55 stars that belong to Trumpler 27, their coordinates and V_o magnitudes are as given in table 5.3. The apparent magnitudes were de-reddened using standard reddening law. The list consist of all the spectroscopically observed stars and the selected ones except 010, 043, 006, and 022.

Table 5.3: Co-ordinates and V_o magnitudes of Trumpler 27 stars

RA(J2000)	**Dec(J2000)**	V_o **Mag**
264.0604	-33.488	4.420
264.1248	-33.4428	6.640
263.8585	-33.6481	3.049
264.0829	-33.4368	6.910
264.0405	-33.5152	6.140
264.0843	-33.432	8.299
264.0733	-33.4684	8.924
264.0535	-33.4886	4.120
264.0724	-33.5006	9.331
264.1142	-33.4933	5.180
264.1568	-33.4562	6.190
264.055	-33.4845	8.440
264.3096	-33.5317	10.35
264.0924	-33.5197	7.330
264.1146	-33.4878	9.344
263.8401	-33.3954	10.19
264.1202	-33.4873	10.73
264.0421	-33.4932	8.330
264.0778	-33.5674	11.04
263.9505	-33.3431	9.330
263.9737	-33.6767	10.34
263.9262	-33.6119	10.47
264.0537	-33.4862	8.496
263.8883	-33.4527	10.37
264.2539	-33.5546	8.611
264.2833	-33.561	10.36
264.0449	-33.48	6.300
264.0909	-33.4763	9.988
264.0973	-33.5292	7.050
264.2533	-33.3857	10.31
264.2095	-33.5492	10.13
264.134	-33.5305	10.07
263.9056	-33.4864	9.789
263.9394	-33.6208	10.26
264.3447	-33.5714	9.602
264.0657	-33.5783	9.881
264.3033	-33.606	10.08
264.0542	-33.481	9.181
264.1322	-33.671	7.832
264.0795	-33.3776	10.43
264.0793	-33.5236	8.761
264.0436	-33.5007	8.850
264.1015	-33.5528	7.260
264.2402	-33.4967	9.896
264.0736	-33.6098	8.002
264.2167	-33.3711	10.09
264.2912	-33.6818	8.644
264.1381	-33.3102	7.644
264.1506	-33.5163	9.811
264.1052	-33.519	8.394
264.0694	-33.2809	7.990
264.2687	-33.4204	9.376
264.0694	-33.6361	7.999
264.1476	-33.5035	9.387
264.0421	-33.3721	8.623

Chapter 6

Conclusion

Our spectroscopic and photometric study of Trumpler 27 reveal that it is a young cluster made up of ~ 55 stars down to a magnitude limit of 15 located at a distance of $\sim 2.6 \pm 0.2$ kpc. The field of this cluster was found to be affected by background stars and variable reddening. Two plots (figures 5.8 and 5.10) show clear evidence that Trumpler 27 exists and is not just a gap in the extinction. The two plots confirm that a young cluster exists in the field. The radial velocities of the cool supergiants also gave a clear indication that Trumpler 27 is a cluster whose $RV_{LSR} \sim 18.5 \pm 2$ km/s.

The refined selection methods applied in identifying Trumpler 27 stars from the stars in its field suggest (especially Figure 5.12) that there is a population of stars behind it. It is not clear if these two populations along the cone of sight are indeed separate or whether it is another effect of variable reddening making the background stars appear as a cluster. The majority of OB stars in the population are later type and fainter compared to Trumpler 27 ones. The group is right behind Trumpler 27 which makes it difficult to separate its members from Trumpler 27 ones with precision. A deeper spectroscopic search for MS stars of both populations should be done to assist in understanding them further. It is proposed that RVs of BSGs and a few OB dwarfs in the field be estimated in the future to give a more complete picture about the two populations.

Our work shows that Trumpler 27 consists of coeval MS, blue supergiants and cool supergiants stars. It is not clear if WR95 and the other WR star in the field (Tr27-105) are part of the cluster as noted earlier from the age gap, but given the derived distance of the cluster and those of the WR stars (WC9 at 2.8 and Tr27-105 at 2.4 kpc respectively as derived by Conti & Vacca 1990), one may think that they belong to it.

The cluster is centred at $\alpha \sim 264.1^o$ & $\delta \sim -33.5^o$ and covers an area of $\sim 13'$ by $11'$. The different methods applied in estimating the cluster distance and age gave different distances and ages ranging from ~ 2.1 kpc to 2.6 kpc and $\sim 10^{6.6-7.2}$ years respectively. The distance ($\sim 2.6 \pm 0.2$) kpc and age ($\sim 10^{7.0 \pm 0.2}$) years derived from optical CMD (figure 5.14) are adopted as our final result.

Trumpler 27 has drawn lots of interest from authors due to its uniqueness. The interests

are due to views about its existence, its distance, age, membership and reddening. Two authors do not believe that the cluster exists (Perren et al. 2012, Imhoff & Keenan 1976), which is contrary to our finding. Three authors, Moffat et al. (1977), Massey (2003) & Perren et al. (2012) did detailed studies on this cluster and derived different distances (see section 3.2) for the cluster. Our distance and reddening agree well with Massey (2003)'s and Moffat et al. (1977)'s respectively. We also find that the stellar over density region noted by Perren et al. (2012) exist and is most likely another cluster.

The study of Trumpler 27 poses a lot of challenges with the major one being estimation of its distance due variable reddening. The different methods of estimating its distance seem to agree with small variations with the nearest reliable estimate being $\sim$ 2.1 kpc and the farthest as $\sim$ 2.6 kpc. The distance estimated from $V - M_V$ vs $E(B - V)$ plot was ignored as unreliable since it is not clear if the star chosen as the least reddened one in the cluster is indeed the least reddened. Since this method relies heavily on a single star, it may be inaccurate.

Optical Q parameter and the evolutionary deviation curve are powerful tools in the study of open clusters affected by variable reddening and should be used more regularly since they reveal clustering behaviour even in variably reddened fields (Figures 5.8 & 5.10). Q parameter should though be used with care to avoid inclusion of late type stars during selection of cluster members which complicates analysis of cluster fields Figure 5.9.

The importance of studying open clusters is to aid in accurate mapping of the Galaxy. If more clusters are studied and their distances accurately estimated, then the map of the Galaxy will be highly improved. A combination of HII regions, open clusters, together with, masers, red giant clump and cepheids allow for more accurate mapping of the Galaxy (Feast 2013). The recently launched Gaia satellite (Jackson et al. 2015) will measure proper motions and radial velocities for $\sim$ 1 billion stars, providing an unprecedented map of the Milky way.

Bibliography

Alpaslan, M. 2009, ArXiv e-prints, 0912.4755

Andrillat, Y., Jaschek, C., & Jaschek, M. 1995, A&AS, 112, 475

Ashman, K. M. & Zepf, S. E. 2001, AJ, 122, 1888

Bakker, R. & The, P. S. 1983, A&AS, 52, 27

Balser, D. S., Rood, R. T., Bania, T. M., & Anderson, L. D. 2011, ApJ, 738, 27

Bania, T. M., Anderson, L. D., Balser, D. S., & Rood, R. T. 2010, ApJ, 718, L106

Binney, J. & Merrifield, M. 1998, Galactic Astronomy (Princeton University Press)

Borissova, J., Bonatto, C., Kurtev, R., Clarke, J. R. A., Peñaloza, F., Sale, S. E., Minniti, D., Alonso-García, J., Artigau, E., Barbá, R., Bica, E., Baume, G. L., Catelan, M., Chenè, A. N., Dias, B., Folkes, S. L., Froebrich, D., Geisler, D., de Grijs, R., Hanson, M. M., Hempel, M., Ivanov, V. D., Kumar, M. S. N., Lucas, P., Mauro, F., Moni Bidin, C., Rejkuba, M., Saito, R. K., Tamura, M., & Toledo, I. 2011, A&A, 532, A131

Bradt, H. 2003, Astronomy Methods (Cambridge University Press)

Bressan, A., Marigo, P., Girardi, L., Salasnich, B., Cero, C., Rubele, S., & Nanni, A. 2012, MNRAS, 427, 127

Camargo, D., Bonatto, C., & Bica, E. 2015, MNRAS, 450, 4150

Cardelli, J. A., Clayton, G. C., & Mathis, J. S. 1989, ApJ, 345, 245

Carroll, B. W. & Ostlie, D. A. 2006, An introduction to modern astrophysics and cosmology, 2nd edn. (San Francisco: Pearson, Addison-Wesley)

Celis, L. 1981, A&A, 99, 58

Cenarro, A. J., Cardiel, N., Gorgas, J., Peletier, R. F., Vazdekis, A., & Prada, F. 2001, MNRAS, 326, 959

Conti, P. S. & Vacca, W. D. 1990, AJ, 100, 431

Coppola, G., Dall'Ora, M., Marconi, M., Musella, I., Ripepi, V., Bono, G., Caputo, F., Corsi, C. E., Piersimoni, A. M., & Storm, J. 2012, Memorie della Societa Astronomica Italiana Supplementi, 19, 190

Cutri, R. M., Skrutskie, M. F., van Dyk, S., Beichman, C. A., Carpenter, J. M., Chester, T., Cambresy, L., Evans, T., Fowler, J., Gizis, J., Howard, E., Huchra, J., Jarrett, T., Kopan, E. L., Kirkpatrick, J. D., Light, R. M., Marsh, K. A., McCallon, H., Schneider, S., Stiening, R., Sykes, M., Weinberg, M., Wheaton, W. A., Wheelock, S., & Zacarias, N. 2003, VizieR Online Data Catalog, 2246

Deharveng, L., Lefloch, B., Kurtz, S., Nadeau, D., Pomarès, M., Caplan, J., & Zavagno, A. 2008, A&A, 482, 585

Dias, W. S., Alessi, B. S., Moitinho, A., & Lépine, J. R. D. 2002, A&A, 389, 871

Drilling, J. S. & Landolt, A. U. 2000, Normal Stars (New York: AIP Press), 381

Ekstrom, S., Georgy, C., Eggenberger, P., Meynet, G., Mowlavi, N., Wyttenbach, A., Granada, A., Decressin, T., Hirschi, R., Frischknecht, U., Charbonnel, C., & Maeder, A. 2011, VizieR Online Data catalog, 353, 70146

—. 2012, A&A, 537, A146

Elmegreen, B. G. & Efremov, Y. N. 1998, astro-ph/9801071

Feast, M. W. 2013, Galactic Distance Scales, Vol. 5 (Springer Science), 829

Fitzgerald, M. P. 1970, A&A, 4, 234

Goetz, P. W. 1991, The New Encyclopaedia Britannica, 15th edn. (Encyclopaedia Britannica)

Gomez, M., Hartmann, L., Kenyon, S. J., & Hewett, R. 1993, AJ, 105, 1927

Gozha, M. L., Borkova, T. V., & Marsakov, V. A. 2012, Astronomy Letters, 38, 506

Gray, R. O. & Corbally, J., C. 2009, Stellar Spectral Classification (Princeton University Press)

Gutierrez-Moreno, A. 1975, PASP, 87, 805

Huyan, Z.-B., Zhu, Z., & Liu, J.-C. 2015, Research in Astronomy and Astrophysics, 15, 393

Imhoff, C. L. & Keenan, P. C. 1976, ApJ, 205, 455

Jackson, P. D., Fitzgerald, M. P., & Moffat, A. F. J. 1980, A&AS, 41, 211

Jackson, R. J., Jeffries, R. D., Lewis, J., Koposov, S. E., Sacco, G. G., Randich, S., Gilmore, G., Asplund, M., Binney, J., Bonifacio, P., Drew, J. E., Feltzing, S., Ferguson, A. M. N., Micela, G., Neguerela, I., Prusti, T., Rix, H.-W., Vallenari, A., Alfaro, E. J., Allende Prieto, C., Babusiaux, C., Bensby, T., Blomme, R., Bragaglia, A., Flaccomio, E., Francois, P., Hambly, N., Irwin, M., Korn, A. J., Lanzafame, A. C., Pancino, E., Recio-Blanco, A., Smiljanic, R., Van Eck, S., Walton, N., Bayo, A., Bergemann, M., Carraro, G., Costado, M. T., Damiani, F., Edvardsson, B., Franciosini, E., Frasca, A., Heiter, U., Hill, V., Hourihane, A., Jofré, P., Lardo, C., de Laverny, P., Lind, K., Magrini, L., Marconi, G., Martayan, C., Masseron, T., Monaco, L., Morbidelli, L., Prisinzano, L., Sbordone, L., Sousa, S. G., Worley, C. C., & Zaggia, S. 2015, A&A, 580, A75

Jaschek, C. & Jaschek, M. 1987, S&T, 74, 612

Johnson, H. L. 1960, Lowell Observatory Bulletin, 5, 17

Johnson, H. L. & Morgan, W. W. 1953, ApJ, 117, 313

Karttunen, H., Krüger, P., Oja, H., Poutanen, M., & Donner, K. J., eds. 2007, Fundamental Astronomy (Berlin: Springer)

Keenan, P. C. & McNeil, R. C. 1989, ApJS, 71, 245

Kharchenko, N. V., Scholz, R. D., Piskunov, A. E., Röser, S., & Schilbach, E. 2007, Astronomische Nachrischten, 328, 889

Kipper, T. 2008, Baltic Astronomy, 17, 311

Kirk, H., Offner, S. S. R., & Redmond, K. J. 2014, MNRAS, 439, 1765

Kirkpatrick, J. D., Henry, T. J., & McCarthy, Jr., D. W. 1991, ApJS, 77, 417

Kronberger, M., Teutsch, P., Alessi, B., Steine, M., Ferrero, L., Graczewski, K., Juchert, M., Patchick, D., Riddle, D., Saloranta, J., Schoenball, M., & Watson, C. 2006, A&A, 447, 921

Lada, C. J. & Lada, E. A. 2003, ARA&A, 41, 57

Leblanc, F. 2010, An Introduction to Stellar Astrophysics (Wiley)

Maeder, A. & Meynet, G. 1987, A&A, 182, 243

Massey, P. 2003, ARA&A, 41, 15

Massey, P., DeGioia-Eastwood, K., & Waterhouse, E. 2001, AJ, 121, 1050

Mermilliod, J. C. 1981, A&A, 97, 235

Mermilliod, J. C., Mayor, M., & Udry, S. 2008, A&A, 485, 303

Minniti, D., Lucas, P. W., Emerson, J. P., Saito, R. K., Hempel, M., Pietrukowicz, P., Ahumada, A. V., Alonso, M. V., Alonso-Garcia, J., Arias, J. I., Bandyopadhyay, R. M., Barbá, R. H., Barbuy, B., Bedin, L. R., Bica, E., Borissova, J., Bronfman, L., Carraro, G., Catelan, M., Clariá, J. J., Cross, N., de Grijs, R., Dékány, I., Drew, J. E., Fariña, C., Feinstein, C., Fernández Lajús, E., Gamen, R. C., Geisler, D., Gieren, W., Goldman, B., Gonzalez, O. A., Gunthardt, G., Gurovich, S., Hambly, N. C., Irwin, M. J., Ivanov, V. D., Jordán, A., Kerins, E., Kinemuchi, K., Kurtev, R., López-Corredoira, M., Maccarone, T., Masetti, N., Merlo, D., Messineo, M., Mirabel, I. F., Monaco, L., Morelli, L., Padilla, N., Palma, T., Parisi, M. C., Pignata, G., Rejkuba, M., Roman-Lopes, A., Sale, S. E., Schreiber, M. R., Schröder, A. C., Smith, M., , Jr., L. S., Soto, M., Tamura, M., Tappert, C., Thompson, M. A., Toledo, I., Zoccali, M., & Pietrzynski, G. 2010, ArXiv e-prints, 15, 433

Moffat, A. F. J., Fitzgerald, M. P., & Jackson, P. D. 1977, ApJ, 215, 106

Negueruela, I., Marco, A., González-Fernández, C., Jiménez-Esteban, F., Clark, J. S., Garcia, M., & Solano, E. 2012, A&A, 547, A15

Nemiroff, R. J. & Bonnell, J. T. 1995, American Astronomical Society, 27, 1291

Nidever, D. L., Marcy, G. W., Butler, R. P., Fischer, D. A., & Vogt, S. S. 2002, ApJS, 141, 503

O'Leary, R. M., Stahler, S. W., & Ma, C.-P. 2014, MNRAS, 444, 80

Padmanabhan, T. 2001, Theoretical Astrophysics - Volume 2, Stars and Stellar Systems (Cambridge University Press)

Perren, G., Vázquez, R. A., & Carraro, G. 2012, A&A, 548, A125

Ramírez Alegría, S., Marín-Franch, A., & Herrero, A. 2012, A&A, 541, A75

Sharpless, S. 1959, ApJS, 4, 257

Sung, C. K. 2006, Journal of Korean Astronomical Society, 39, 1

The, P. S. & Stokes, N. 1970, A&A, 5, 298

Tonry, J. & Davis, M. 1979, AJ, 84, 1511

Turner, D. G. 1973, AJ, 78, 597

van Bueren, H. G. 1952, Bull. Astron. Inst. Netherlands, 11, 385

van der Hucht, K. A. 2001, New Astronomy Reviews, 45, 135

Van Genderen, A. M. 1980, A&A, 88, 77

Van Genderen, A. M. & Thé, P. S. 1978, A&A, 64, L1

Verheyen, L., Messineo, M., & Menten, K. M. 2012, A&A, 541, A36

Walborn, N. R. & Fitzpatrick, E. L. 1990, PASP, 102, 379

Wallerstein, G., Westbrooke, W., & Hannibal, D. 1963, PASP, 75, 522

Wegner, W. 2006, MNRAS, 374, 1549

Zhao, J. L. 2007, Progress in Astronomy, 25, 13